10 Connected rings

10.1 Quantized conductance

For a short introduction into the phenomenon of quantized conductance see Section 7.1.2 on page 118.

Ismail et al [91I2, 91L1] (page 270) measured the conductance of GaAs rings and observed a step–like behaviour as a function of gate voltage at 4.2 K. When recycling the gate bias, the threshold voltage shifted by ≈ 50 mV, the heights of the steps were unaltered. In a single ring, the height of the steps was $0.8 \cdot e^2/h$, in a two–loop sample it was $1.2 \cdot e^2/h$ (Fig. 273). Similar steps were observed in $2-4\,\mu$m long single wires as well as in ten parallel wires. The step heights in the single wires were $2 \cdot e^2/h$ and $20 \cdot e^2/h$ in the parallel wires.

Jin et al [92J2] (see page 119) fabricated wires (minimum width below 40nm) and rings from poly–crystalline Si by EBL and dry etching and observed quantized conductance.

Liu et al [93L3] (page 275) observed regularly spaced conductance steps in GaAs rings (Fig. 283). The average height of the steps was $0.75 \cdot e^2/h$.

Gao et al [94G1] (page 272) observed conductance steps at ≈ 1 K in an array of four parallel rings made of a Si/SiGe heterostructure (Fig. 277). The steps were not exactly equally spaced, their origin was not absolutely clear.

10.2 Finite temperature

Finite temperature leads to energy evaraging of AB interference patterns (see Section 10.6.2 on page 264). Within some band width, E_c, the neighbouring levels are spatially correlated and for $k_B T < E_c$, only the fundamental AB interference pattern contributes to the conductance. When $k_B T > E_c$, $N = k_B T/E_c$ uncorrelated bands are summed to give the final pattern and the amplitude of the periodic h/e oscillations shrinks proportional to $N^{-1/2} \propto T^{-1/2}$. (A similar reduction of the signal occurs when the voltage drop across the sample is larger than E_c/e.) The $h/2e$ oscillations due to time reversed paths do not decrease in amplitude when averaged over an energy range $k_B T$. Further, the phase coherence length decreases with increasing temperature and when l_φ becomes smaller than L, the AB and the weak–localization oscillations decay exponentially with temperature due to dephasing (see for example [86W1, 92W1] and references therein and Section 7.3.4 on page 138).

Chang et al [88C5] (page 266) studied the temperature dependence of h/e AB oscillations and AF. The amplitude of AF and QF in R_L followed roughly a $T^{-0.75\pm0.25}$ law between 150 mK and 4 K. Further, the relative size of the AF and the QF component in R_L in comparison with a negative MR peak depended on temperature. At high T, the negative MR peak was favoured. The phase coherence length was $0.66 \cdot (T/2\,K)^{-0.35}\,\mu$m.

Aihara et al [91A3] studied the temperature dependence of the phase coherence length in a device fabricated by EBL and RIE on modulation–doped AlGaAs/GaAs heterostructures grown by MBE. The loop was elliptic with an average diameter of $1.25\,\mu$m, a structural width of $0.5\,\mu$m, and an effective linewidth of $0.17\,\mu$m. The elastic scattering length was $2.0\,\mu$m. The ring had about 16 transverse modes. MR data for various temperatures are shown in Fig. 246. In the Fourier transform of the data at 0.75 K (Fig. 247), peaks corresponding to h/e and $h/2e$ oscillations were present. The Fourier periods were independent of temperature. The temperature dependence of the amplitude of the AB oscillations is illustrated in Fig. 248. The values of l_φ as a function of temperature were extracted and results are shown in Fig. 249. The behaviour of the phase coherence time was approximately proportional to T^{-2} above 2.0 K.

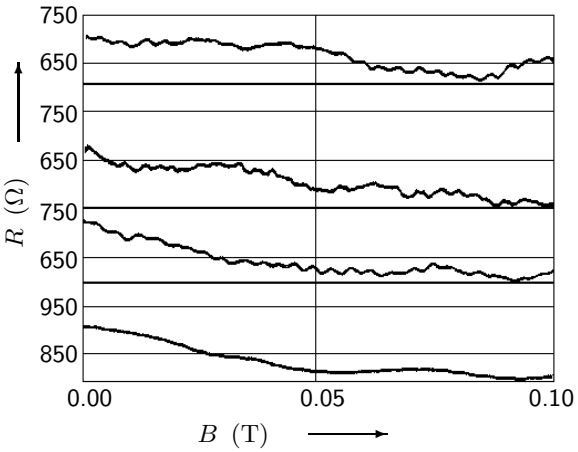

Fig. 246: MR of a GaAs ring [91A3] at (top) $T =$ 0.45 K, 0.75 K, 1.7 K, and 4.2 K (bottom).

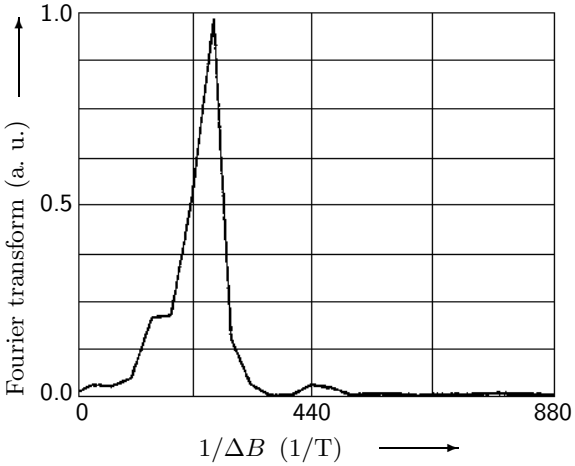

Fig. 247: Fourier power spectrum of the MR of Fig. 246 at 0.75 K. Two peaks corresponding to h/e (at $\approx 270\,\mathrm{T}^{-1}$) and $h/2e$ (at $\approx 400\,\mathrm{T}^{-1}$) oscillations are visible.

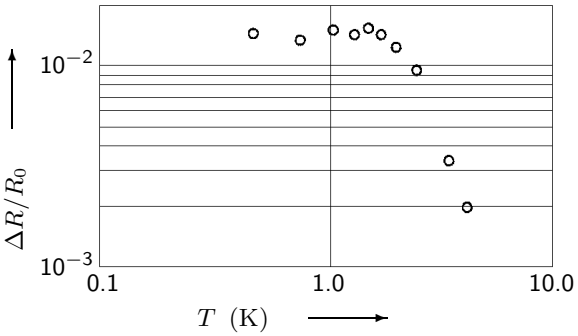

Fig. 248: Temperature dependence of the AB oscillation amplitude [91A3]. Vertical axis is the ratio of the peak–to–peak oscillation amplitude, ΔR, and the zero magnetic field resistance, R_0.

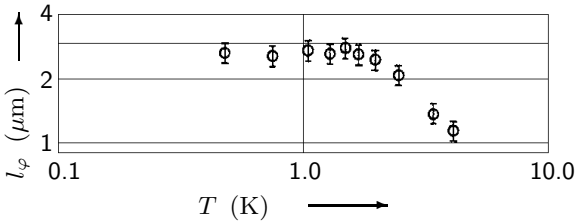

Fig. 249: Temperature dependence of the phase coherence length [91A3].

Kurdak et al [92K1] studied interference effects in rings and wire arrays of $GaAs/Al_{0.3}Ga_{0.7}As$ and pseudomorphic $Ga_{0.2}In_{0.8}As/Al_{0.48}In_{0.52}As$ modulation–doped heterostructures. MR data for a 7.8 μm perimeter ring of GaAs and a 5.2 μm perimeter ring of GaInAs at different temperatures are shown in Figs. 250 and 251. The AB oscillations had the expected h/e period. The phase coherence length in the pseudomorphic GaInAs rings seemed to be longer than in the other samples as AB oscillations were observable up to 19 K in comparison with 4 K in the GaAs rings. The peak position in the MR did not vary with temperature. The AB conductance amplitude as a function of T for four different rings of GaAs is illustrated in Fig. 252. The amplitudes of the AB oscillations were smaller for rings with a larger perimeter and decreased with increasing temperature. The phase coherence length as a function of temperature was extracted from the amplitudes of the AB oscillations. It turned out that $l_\varphi \approx 1.5 - 4\,\mu$m was smaller than the perimeters of the rings in the temperature range of the experiment. Further, l_φ was deduced from weak–localization measurements in parallel wires.

Chandrasekhar et al [94C1] (page 275) investigated InO rings and found periodic oscillations of conductance as a function of gate voltage. The oscillations persisted up to temperatures of 12 K in

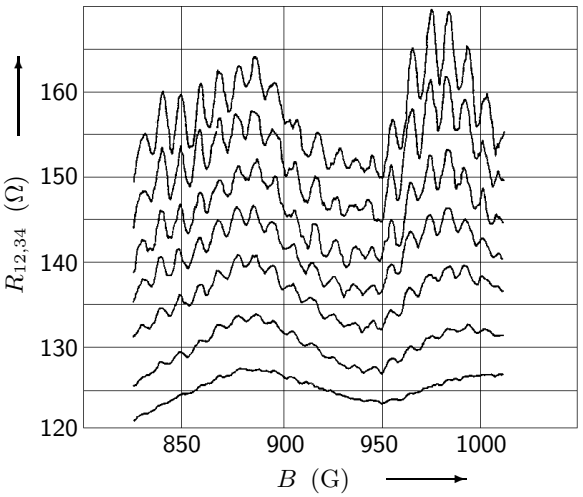

Fig. 250: Four–terminal resistance $R_{12,34}$ [92K1] vs. magnetic field at (top) $T = 0.41\,\mathrm{K}$, $0.58\,\mathrm{K}$, $0.94\,\mathrm{K}$, $1.3\,\mathrm{K}$, $1.8\,\mathrm{K}$, $2.5\,\mathrm{K}$, and $4.2\,\mathrm{K}$ (bottom) for the $7.8\,\mu$m perimeter ring of GaAs. The y-axis is given for the $4.2\,\mathrm{K}$ data, the other curves are displaced by $10\,\Omega$ from each other.

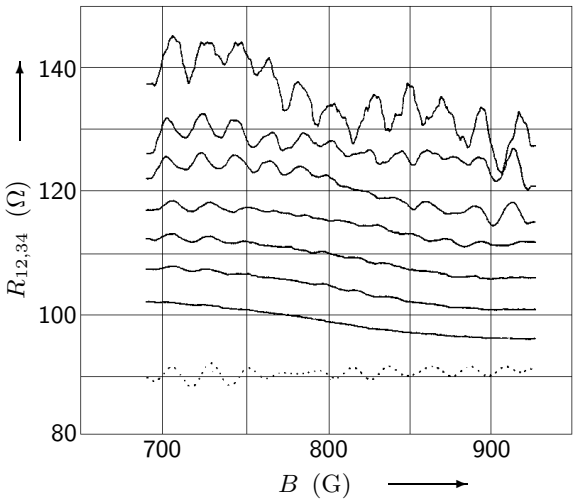

Fig. 251: Four–terminal resistance of the $5.2\,\mu$m perimeter sample of GaInAs. The temperatures are (top) $0.4\,\mathrm{K}$, $1.5\,\mathrm{K}$, $3.5\,\mathrm{K}$, $7.0\,\mathrm{K}$, $9.4\,\mathrm{K}$, $12\,\mathrm{K}$, and $19\,\mathrm{K}$ (solid curve at the bottom). The y-axis is given for the $19\,\mathrm{K}$ data; the other curves are displaced by $5\,\Omega$ from each other. The dashed line shows the $19\,\mathrm{K}$ data after the background resistance has been substracted and it has been magnified by a factor of 20.

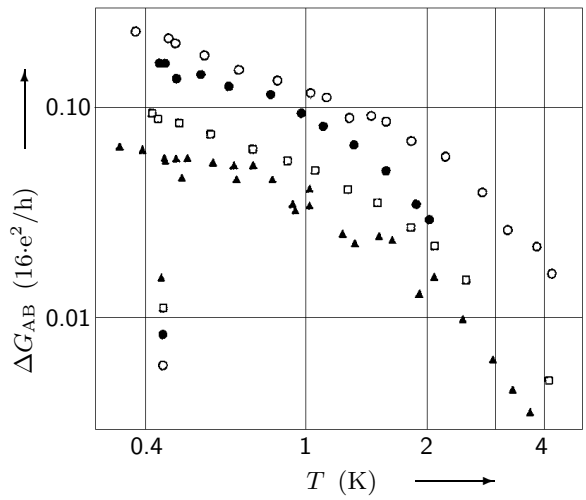

Fig. 252: AB MC amplitude ΔG_{AB} vs. temperature for four rings of perimeters $8.8\,\mu$m (triangles), $7.8\,\mu$m (boxes), $6.7\,\mu$m (solid circles), and $5.2\,\mu$m (open circles) of the GaAs sample [92K1].

some samples. When the temperature decreased, the amplitudes of the minima of the oscillating conductance vanished while the amplitudes of the maxima were at first reduced and then became relatively constant at low temperatures (Fig. 286). The period of oscillation did not change with temperature. In some samples, the amplitude of some peaks decreased that fast when temperature was lowered that the oscillation pattern appeared to be aperiodic (Fig. 287).

Appenzeller et al [95A2] investigated the inelastic mean free path as a function of temperature in rings of small width in a strained $In_{0.77}Ga_{0.23}As/InP$ system. The rings were patterned by EBL and RIE and had widths of about 85 nm and average diameters of 0.7 μm. The elastic mean free path was 4.7 μm. The four–terminal MR, R_L, as a function of magnetic field at 330 mK is shown in Fig. 253. The AB oscillations had an amplitude of 1 kΩ on a background resistance of 8.5 kΩ. From the width of the h/e peak in the Fourier spectrum, an inner ring diameter of 648 nm and an outer diameter of 819 nm were inferred. A $h/2e$ peak was a second harmonic AB oscillation. Both periods were independent of T in the temperature range investigated. From AF in the background resistance a phase coherence length of 1.1 ± 0.12 μm was deduced. The AB oscillations were decreasing in amplitude for an increasing magnetic field and vanished at $\approx$ 1.2 T. Appenzeller et al assumed the main contribution to the phase coherence length to be due to electron–electron scattering and studied the AB effect as a function of temperature and of the current through the ring, corresponding to an excess energy $\tilde{\Delta}$ above E_F (Fig. 254). The AB oscillations at 10 nA and 330 mK died out if either temperature or the excess energy were enhanced. The phase coherence length was deduced from the T– and the $\tilde{\Delta}$–dependent data. There was a maximum in the saturation value of l_φ around 1.1 μm which was reached for an excess energy of 0.1 meV. Further reducing the excess energy did not enhance l_φ.

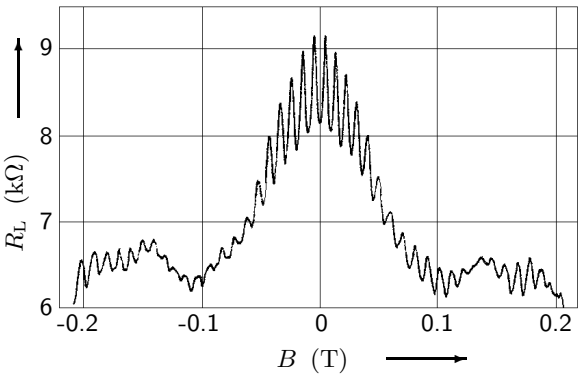

Fig. 253: MR of an $In_{0.77}Ga_{0.23}As/InP$ ring [95A2] vs. magnetic field normal to the ring at $T = 0.33$ K and for $I = 1$ nA.

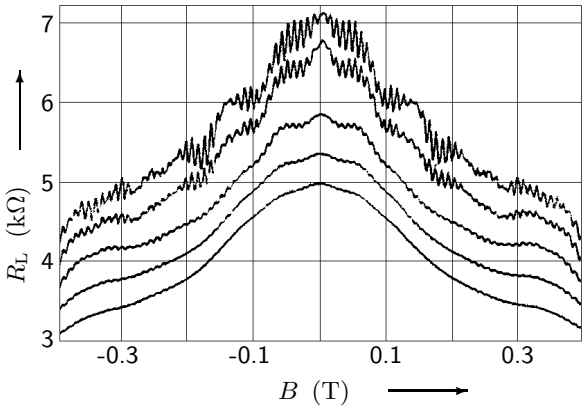

Fig. 254: R_L vs. magnetic field at $I = 10$ nA for (top) $T = 0.33$ K, 2 K, 5 K, 7 K, and 10 K (bottom) [95A2]. The curves have been vertically offset for clarity by a value of 300 Ω.

Kvon et al [98K6] studied quantum corrections to the conductance of a quasi–ballistic GaAs ring ($w = 0.4$ μm, $w_{eff} = 50 - 100$ nm, $L \approx 2$ μm, $l = 2.8$ μm), fabricated by EBL and plasma etching. The conductance as a function of temperature decreased with increasing T for $T > 15$ K due to phonon scattering and increased with increasing T for $2\,\mathrm{K} < T < 15\,\mathrm{K}$. The behaviour of conductance with temperature in the latter region was attributed to WL. The correction ΔG followed $T^{-1/2}$ (as predicted theoretically for diffusive wires) for $T > 6$ K, while for $T < 6$ K the data was sensitive to temperature changes, which was attributed to a cross–over from 1D behaviour to 0D behaviour. The phase coherence length was determined via MR measurements, also AB oscillations were observed.

10.3 Sample geometry

10.3.1 Width and length

For a general introduction see Section 7.4.1 on page 144. In the case of AB oscillations (see Section 10.6.2 on page 264), the period of the oscillations is determined by the area the current encloses. In a ring of finite width, current loops with different areas contribute to the interference pattern. Hence, the peaks in the Fourier transform of the MR data have finite widths and changing the width of the ring affects the width of the Fourier peaks. Further, the amplitude of the AB oscillations decreases exponentially when the distance between the voltage probes increases such that $L > l_\varphi$.

Ford et al [88F3] studied rings made from GaAs/AlGaAs heterojunctions. A Schottky gate was formed in order to deplete the 2DEG and a ring was defined at a gate voltage of $V_g = -0.36 \pm 0.01$ V. The conducting channels pinched off at $V_g \approx -2.3$ V. The width of the channels could be varied from 900 down to $\approx 150 \pm 50$ nm. AB oscillations for different gate voltages are shown in Fig. 255. The Fourier transform of the data is displayed in Fig. 256. The h/e peak became narrower for a decreasing channel width. The oscillations did not decrease in amplitude up to fields between 0.5 and 1 T depending on the channel width. Another consequence of the narrowing of the channels can be seen when plotting the Landau level index corresponding to each minimum in the MR, n_L, versus $1/B$ (Fig. 257). The lines bent down at high values of n_L, the bending increased as the channel was narrowed.

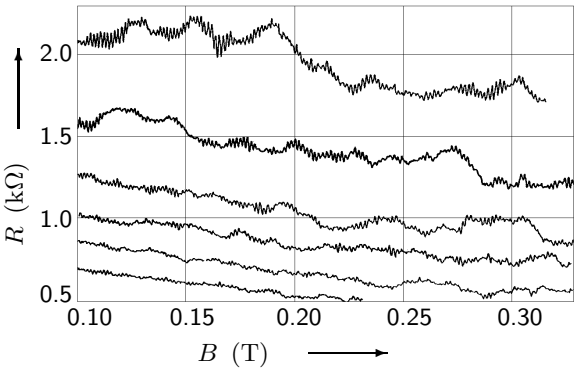

Fig. 255: MR of a GaAs ring [88F3] for (top) $V_g = -2.0$ V, -1.9 V, -1.8 V, -1.7 V, -1.6 V, and -1.5 V (bottom). The h/e period was 1.6 mT.

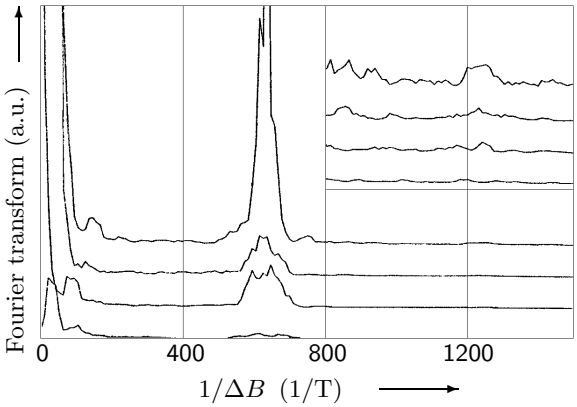

Fig. 256: Fourier transform of the data in Fig. 255 after substraction of the background for (top) $V_g = -2.0$ V, -1.9 V, -1.8 V, -1.6 V (bottom). The h/e peak located at $\approx 600\,\mathrm{T}^{-1}$ corresponded to a loop of average radius 0.9 μm. The curves have been offset for clarity. The inset displays the region around $1200\,\mathrm{T}^{-1}$ multiplied by 10 in order to show the $h/2e$ peak (at $\approx 1250\,\mathrm{T}^{-1}$).

Ford et al [89F3] reported relative amplitudes of AB oscillations as large as 20% in a GaAs ring defined by electrostatic confinement. The width of the conducting channels could be varied via V_g. Ford et al found AB oscillations with a period of ≈ 2 mT. The relative amplitude of the AB oscillations increased with decreasing channel width, the optimum results were a $\Delta R/R$ of 18% at $V_g = -1.076$ V and of 20% at $V_g = -1.054$ V for small ranges of B. By filtering the MR data, $h/2e$ oscillations were also found, which behaved similar to the h/e oscillations for $B \geq 4$ mT. For smaller magnetic fields, they showed characteristic features of the weak–localization oscillations. The period of the AB oscillations increased sharply as B was swept from zero to ≈ 0.3 T. The

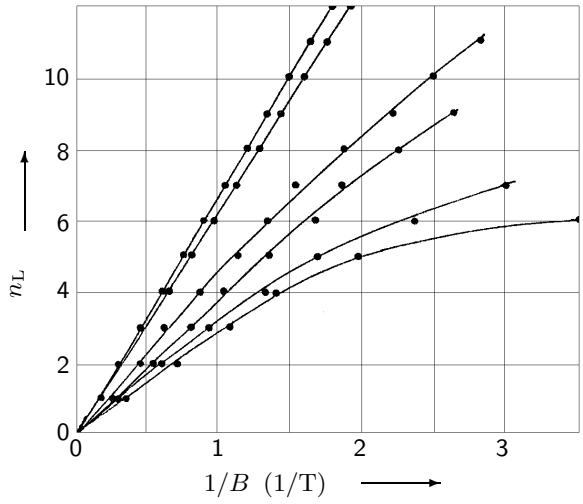

Fig. 257: Fan diagram showing the positions of the minima in the MR plotted vs. inverse magnetic field for (left) $V_g = -0.4\,V$, $-0.9\,V$, $-1.6\,V$, $-1.9\,V$, $-2.0\,V$, and $-2.1\,V$ (right) [88F3]. Full curves are guides to the eye.

overall increase in period was 25% and indicated a decrease in the average area enclosed by the ring. At high fields and for wide channels, the quantum Hall effect was observed with zeroes in R_L and plateaux in R_H.

Kurdak et al [92K1] (page 256) studied interference effects in GaAs/$Al_{0.3}Ga_{0.7}As$ and pseudomorphic $Ga_{0.2}I_{0.8}As/Al_{0.48}In_{0.52}As$ modulation–doped heterostructures. The amplitudes of the AB oscillations were smaller for rings with a larger perimeter.

10.3.2 Special geometries

The geometries investigated in the experiments described in this Section are a double–wire interferometer and a ring with a quantum dot embedded in one arm.

Okuda et al [93O5] observed quantum interference effects in a GaAs/$Al_xGa_{1-x}As$ interferometer consisting of double quantum wires and triple Schottky gates. Both wires were straight and coupled by a thin barrier. The phase of the electron wave function was controlled by tuning the gate voltages. Oscillations in the source–drain resistance as a function of the gate voltage across the main gate were observed. The oscillations had a relative amplitude of 4%.

Okuda [93O4] observed AB oscillations in the MR of a GaAs double–wire interferometer (see [93O5] on page 260). The MR was measured in several samples of which some showed no oscillations, some exhibited sinusoidal oscillation patterns, and others showed oscillations with non–sinusoidal patterns.

Yacoby et al [95Y2] constructed a GaAs ring with a QD embedded in its left side arm. The dot area and the coupling to the ring's arm could be varied by gates. The dot contained about 200 electrons, its resistance was $10^2 - 10^3\,k\Omega$, while the resistance of each arm of the ring was $\approx 5\,k\Omega$. MR was measured at $T = 80\,mK$, AB oscillations were observed (period $\approx 20\,G$), directly indicating that transport through the QD had a coherent component (Fig. 258). AB oscillations for three typical successive CB peaks had all the same phase at the peaks (Fig. 259). Following the phase along a single CB peak, a phase change of π occurred (Fig. 260). This phase change was accompanied by severe noise in the ring's current.

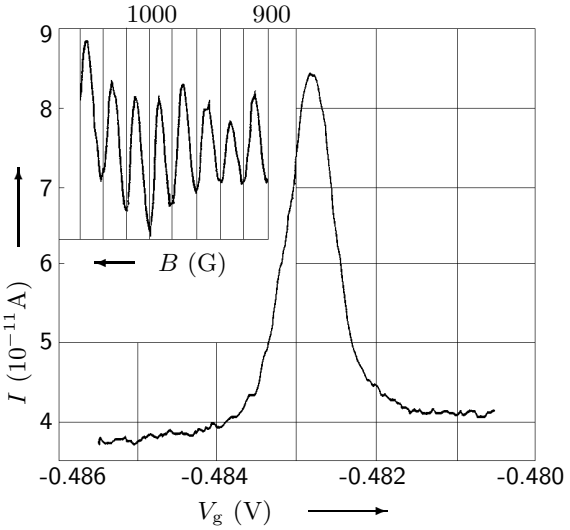

Fig. 258: One of the ring's current peaks as a function of gate voltage [95Y2]. Inset: Current vs. Magnetic field at gate voltage $-0.483\,\mathrm{V}$ showing AB oscillations.

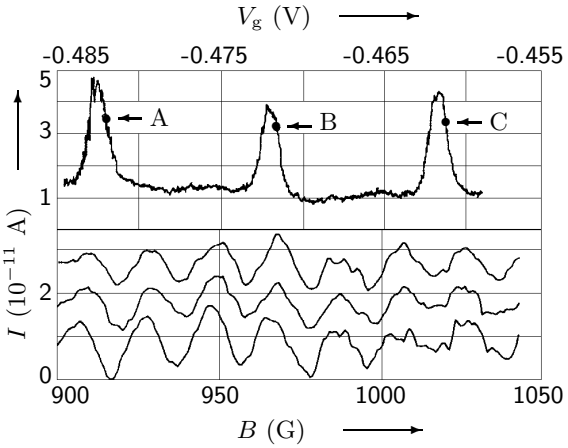

Fig. 259: A series of Coulomb peaks (upper picture) and the corresponding current oscillations taken at the marked points A (lower picture, top curve), B, and C (lower picture, bottom curve) in successive peaks of the ring's current [95Y2].

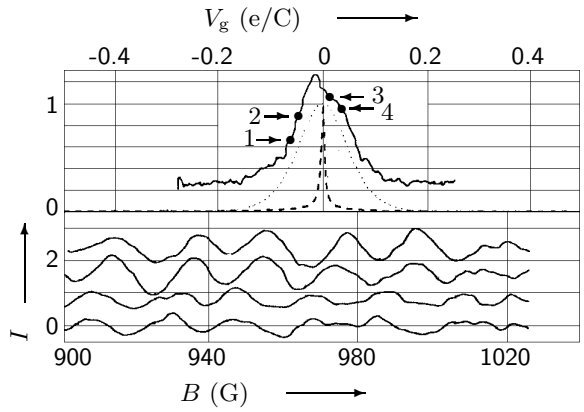

Fig. 260: The evolution of the phase along one conductance peak in arbitrary units (upper picture) [95Y2]: level broadening, Γ, at $T = 0\,\mathrm{K}$ (broken line) and for $k_B T > \Gamma$ (dotted line), and the experimentally measured peak (solid line, shifted up). A series of interference patterns (lower picture) taken at points (bottom) 1, 2, 3, and 4 (top) on a peak. The current is in units 10^{-11} A.

10.4 Impurities

For an introduction into the influence of impurities on transport in mesoscopic conductors see Section 7.5.1 on page 157 and Section 11.1.4 on page 285.

Chandrasekhar et al [94C1] (page 275) investigated InO rings and observed periodic oscillations of conductance as a function of gate voltage. Even though the oscillations were in general reproducible if the sample was kept at low temperature, the conductance of a sample occasionally changed in a discrete way, usually accompanied by a change in the pattern of the oscillations; the period of the oscillations was not affected. Chandrasekhar et al believed the discrete behaviour of the conductance to be due to the movement of isolated impurities.

Bykov et al [96B2] (page 291) investigated in–plane gated InGaAs/AlGaAs rings. The resistance as a function of V_g showed a hysteresis explained by charge exchange of impurities in the vicinity of the 2DEG.

10.5 Interactions

For an introduction into the influence of electron–electron interactions onto transport in small semiconductor devices see Section 7.6.1 on page 162. For literature concerning Berry's phase induced by uniform spin–orbit interaction see for example [84B3, 89S4, 98M].

Chandrasekhar et al [94C1] (page 275) studied InO rings and observed periodic oscillations of conductance as a function of gate voltage. Many of the observed phenomena could be accounted for the physics of the Coulomb blockade.

Appenzeller et al [95A2] (page 258) investigated the inelastic mean free path as a function of temperature in rings of small width in a strained $In_{0.77}Ga_{0.23}As$/InP system. They assumed the main contribution to the phase coherence length to be due to electron–electron scattering.

Morpurgo et al [98M] searched for a manifestation of Berry's phase via a splitting of the frequency of AB oscillations. They fabricated rings (diameter between 0.9 and 2.1 μm, $w = 130 - 170$ nm, $l = 1\,\mu$m) from a AlSb/InAs/AlSb heterostructure, a uniform spin–orbit interaction was present in the rings. The AB effect was measured at 100 mK, conductance fluctuations were also observed and a dip in conductance at small B due to WL. The peak in the Fourier spectrum appeared at h/e, but had a rough shape and was quite broad. A possible splitting could not be resolved. The rings resistance showed switching events due to defects present in the heterostructure. The statistical properties of a set of $R(B)$ curves generated by the switching events was equivalent to those that would be obtained from different microscopic realizations of the same sample. Investigating a Fourier spectrum averaged over ≈ 70 different $R(B)$ curves, a clear splitting of the Fourier peak evolved. Morpurgo et al commented that a connection between splitting of the Fourier peak and spin–orbit interaction was not conclusively established.

10.6 Magnetic field

10.6.1 General

For a general introduction into the influence of a magnetic field onto transport see Section 7.7.1 on page 167. For an introduction into the phenomena of *weak–localization* (causing a negative MR peak at small magnetic fields), *aperiodic conductance fluctuations*, and *Shubnikov–de–Haas* oscillations see Sections 7.7.2, 7.7.3, and 7.7.4 on pages 176, 182, and 194, respectively. With respect to the AB effect (see Section 10.6.2 on page 264), the period of the oscillations changes when the magnetic field becomes strong enough in order for edge channels to form, because this

crossover affects the area enclosed by the current. Further, as backscattering between edge states is suppressed, interference between electrons travelling along different paths around the ring is not possible and the AB oscillations decay for an increasing magnetic field.

Timp et al [87T1, 88T4] (page 264) investigated four–terminal MR in GaAs rings. The Hall resistance plateaux in R_H corresponded to the Landau indices 0, 1, 2, and 3.

Ishibashi et al [87I2] (page 265) reported observation of AB oscillations in a small GaAs ring while a wire fabricated for comparison showed only AF. MR data for a ring with one electrical path broken is shown in Fig. 265, only AF were observed in that case.

Mankiewich et al [88M2] (page 266) measured R_L and R_H in rings fabricated by EBL and RIE in modulation–doped GaAs.

Chang et al [88C5] (page 266) studied MR in a GaAs/AlGaAs heterostructure ring. R_L and R_H at 50 mK are shown in Fig. 268. A large negative MR in R_L was observed for $-0.3\,\mathrm{kG} < B < 0.3\,\mathrm{kG}$ (Fig. 269). At $T = 4\,\mathrm{K}$ and $B = 0\,\mathrm{T}$, the negative MR peak was about 7% larger than the background resistance; at 50 mK it was 90% larger. At higher fields, AF and quasi–periodic fluctuations were observed in R_L, AF were observed in R_H.

Simmons et al [88S3] (see page 168) performed MR measurements on doubly connected rings and standard Hall bridges made from GaAs/Al_xGa_{1-x}As heterostructures. Samples of both geometries showed resistance fluctuations.

Ford et al [88F3] (page 259) studied MR in GaAs rings. The width of the channels could be varied from 900 down to $\approx 150 \pm 50\,\mathrm{nm}$ by a gate. Magnetic depopulation was observed when plotting the Landau level index corresponding to each minimum in the MR, n_L, versus $1/B$ (Fig. 257).

Chang et al [88C1] (see page 201) fabricated GaAs wires and rings by EBL and RIE, measured R_L and R_H as a function of magnetic field and observed AF.

Ford et al [89F3] (page 259) measured MR in a GaAs ring. By filtering the data, $h/2e$ oscillations were found, which showed characteristic features of the weak–localization oscillations for $B \leq 4\,\mathrm{mT}$. At high fields and for wide channels, the quantum Hall effect was observed with zeroes in R_L and plateaux in R_H.

Timp et al [89T7] (page 269) studied the suppression of the AB effect in the quantized Hall regime. The minima observed in R_L corresponded to plateaux in R_H.

Liu et al [93L3] (page 275) studied the dispersion relation in GaAs rings. Via the SdH effect, they obtained the Fermi level as a function of gate voltage. The effective mass as a function of magnetic field was deduced and an enhancement of m^* with B was found.

Chandrasekhar et al [94C1] (page 275) examined InO rings and observed periodic oscillations of conductance as a function of gate voltage. The positions of the conductance maxima with respect to the gate voltage shifted as a function of magnetic field and some of the detailed structure changed (Fig. 288). The period of the oscillations remained constant to within 3% over the entire magnetic field range.

Liu et al [94L2] (page 271) studied four coupled GaAs rings and reported that the phase coherence length increased with B. The amplitude of the h/e AB oscillation, $\langle \Delta G(B) \rangle$, was expected to scale as $Pe^{-\Delta l/l_\varphi}$, with P the interference probability of the two partial waves, and Δl the distance a wave travels before the interference. An increase in $\langle \Delta G(B) \rangle$ with magnetic field indicated an increase in l_φ.

Appenzeller et al [95A2] (page 258) investigated MR in rings of small width in a strained $In_{0.77}Ga_{0.23}As$/InP system and observed AF.

Bykov et al [95B3] structured GaAs rings (with inner diameters of 0.2 μm and outer diameters of 0.8 μm and 1 μm) by EBL and plasma etching. They performed MR measurements for $0\,\mathrm{T} < B < 13\,\mathrm{T}$ at $T < 50\,\mathrm{mK}$. At small B, a negative MR was observed. AB oscillations were superimposed on the negative MR. At large B, the MR exhibited plateaux. The MR for $0.6 < \nu < 0.65$ also exhibited AB oscillations while for $\nu = 1/2$, no MR oscillations were present.

Kvon et al [98K6] (page 258) studied quantum corrections to the conductance of a quasi–ballistic GaAs ring. The phase coherence length was determined via MR measurements, AB oscillations were observed.

Morpurgo et al [98M] (page 262) fabricated rings from a AlSb/InAs/AlSb heterostructure. The AB effect was measured at 100 mK, conductance fluctuations were also observed and a dip in conductance at small B due to WL.

10.6.2 Magnetostatic Aharonov–Bohm effect

Interference between electron paths in a conductor may lead to periodic oscillations of resistance as a function of magnetic field in small rings. Two similar but different mechanism are responsible for these oscillations, namely the *Aharonov–Bohm effect* and *weak localization*. In general, the probability $P(x_\mathrm{i} \to x_\mathrm{f})$ of an electron to move from an initial position x_i to a final position x_f is the square of the sum over the probability amplitudes $q_j e^{i\varphi_j}$ of all possible paths connecting x_i with x_f (labelled by numbers j). In the case of only two paths, it is $P(x_\mathrm{i} \to x_\mathrm{f}) = q_1^2 + q_2^2 + 2q_1 q_2 \cos(\varphi_1 - \varphi_2)$. The last term reflects the interference between the two probability amplitudes. Now, first, consider an ideal 1D ring enclosing a magnetic flux ϕ with two contacts attached opposite to each other at x_i and x_f. The magnetic field be completely restricted to the hole of the ring. Due to the non–zero vector potential along the two possible paths, the probability amplitudes acquire a phase shift, $\Delta\varphi_j = -(e/\hbar) \int \boldsymbol{A}(\boldsymbol{x}) d\boldsymbol{x_j}$. Thus, it depends on the magnitude of the enclosed flux whether the interference at x_f is constructive or destructive and the probability $P(x_\mathrm{i} \to x_\mathrm{f})$ oscillates periodically as a function of ϕ with period $\phi_0 = h/e$ ($c \equiv 1$), implying an oscillating MR. In an ideal ring, the MR has a minimum at zero magnetic field. This effect is called *Aharonov–Bohm* (AB) *effect*, it demonstrates the physical relevance of the vector potential $\boldsymbol{A}$ (see for example [59A, 86W1, 88K1, 88W5, 89W1, 89W2, 90D, 91W2, 92W1, 96K4, 97F, 97I1, 98J1] and references therein).

Second, the probability of a particle to return to its starting point instead of proceeding to x_f is enhanced at zero field, due to constructive interference between the transmission amplitudes of time–reversed paths at x_i, $P(x_\mathrm{i} \to x_\mathrm{i}) = 4q^2$. Such paths are called *Cooperons*. As electrons returning to x_i do not contribute to transport, this mechanism leads to an enhancement of resistance and is called *weak localization* (see also Section 7.7.2 on page 176). In the presence of a magnetic flux through the hole of the ring, the transmission probability oscillates periodically as a function of ϕ with period $h/2e$. This process yields a maximum in the MR at zero magnetic field. In a ring of a non–zero cross-section, the $h/2e$ oscillations die out for magnetic fields $B \geq (h/e)/A_\varphi$, where A_φ is the area over which phase coherence is retained (see for example [86C1, 91W2, 92W1, 97F, 97I1, 98J1] and references therein).

For the occurrence of the AB effect and of weak localization, phase coherence around the loop is vital. When the phase coherence length l_φ becomes smaller than the distance L between the voltage probes, the number of electrons travelling coherently around the ring is exponentially reduced and the conductance oscillations decrease as $\Delta G = \Delta R/R^2(0) \propto e^{-L/l\varphi}$ (see for example [86W1, 97F, 97I1] and references therein).

Timp et al [87T1, 88T4] reported the first observation of the AB effect in semiconducting rings fabricated by EBL and RIE on modulation–doped $GaAs/Al_{0.33}Ga_{0.67}As$ heterostructures grown by MBE. Timp et al measured the four–terminal resistance of three annuli with average diameters of 2.35 ± 0.04, 1.88 ± 0.04, and $0.94 \pm 0.02\,\mu$m. The MR, R_L and R_H, observed at 270 mK in the

middle–sized annulus is displayed in Fig. 261. The Hall resistance plateaux in R_H corresponded to the Landau indices 0, 1, 2, and 3. Examples of the periodic oscillations in R_L in the 2.35 μm diameter annulus are shown in Fig. 262. The period of the high–frequency oscillation of 1.4 mT corresponded to h/e oscillations. In R_H, h/e oscillations have also been found. The amplitudes of the periodic oscillations in the MR at 10 mT were $0.016 \cdot e^2/h$, $0.32 \cdot e^2/h$, and $0.51 \cdot e^2/h$ for the 2.35, the 1.88, and the 0.94 μm diameter ring, respectively. The MR in the small and the middle sized annuli near 150 and 300 mT is shown in Fig. 263. The periodic oscillations were damped as the magnetic field increased. The AB effect seemed to be suppressed when the Larmor radius r_c was $\approx w/2$.

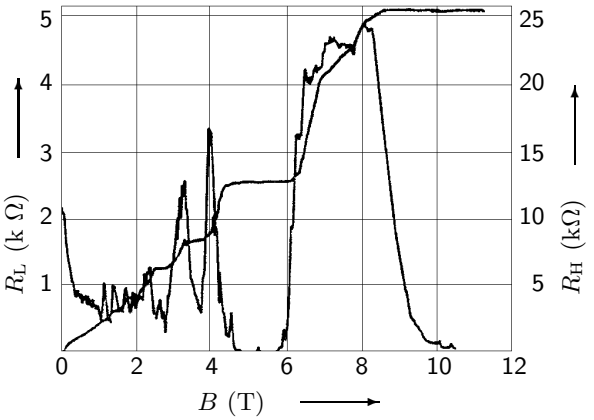

Fig. 261: MR of the middle–sized annulus at 270 mK [87T1]. The curve showing the plateaux is R_H (right axis), the other curve is R_L (left axis).

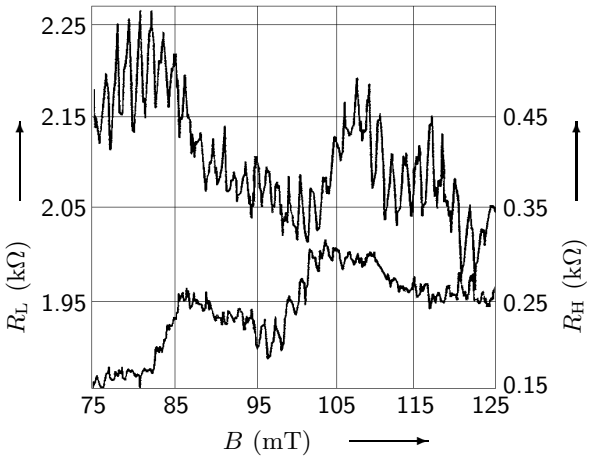

Fig. 262: Periodic MR observed in the large ring [87T1]. Both, R_L and R_H are shown. The left axis corresponds to the upper curve, the right axis to the lower curve.

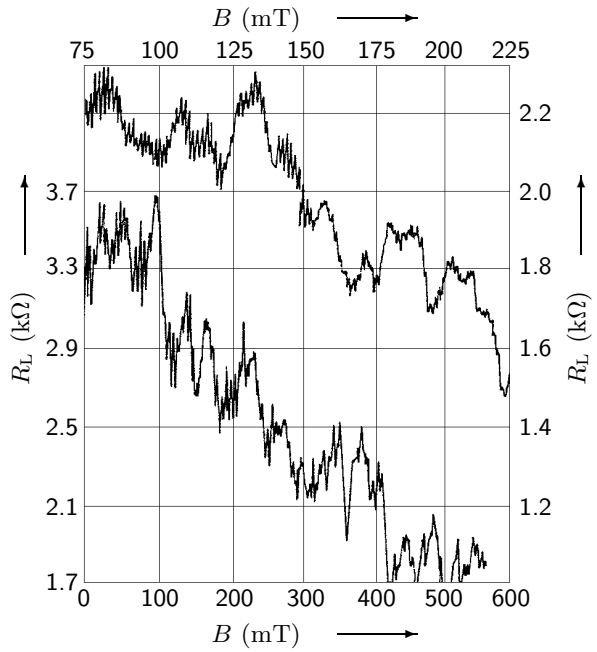

Fig. 263: MR observed in the middle–sized (top, upper and right axes) and the small (bottom, lower and left axes) annuli [87T1].

Ishibashi et al [87I2] reported observation of AB oscillations in a small ring of selectively doped

GaAs/AlGaAs fabricated by EBL and ion etching. A wire fabricated for comparison showed only AF. The inelastic scattering length was smaller than the sample size. The MR of a $1\,\mu$m diameter ring with a linewidth of $0.35\,\mu$m is shown in Fig. 264. The corresponding data for a similar ring but with one electrical path broken is shown in Fig. 265. Only AF were observed in that case. The Fourier transform of the data is displayed in Fig. 266. The peak at $\approx 2.5 \times 10^{-3}\,\mathrm{G}^{-1}$ corresponded to oscillations with a period of h/e. The amplitude of the oscillations was $\approx 0.1 \cdot e^2/h$.

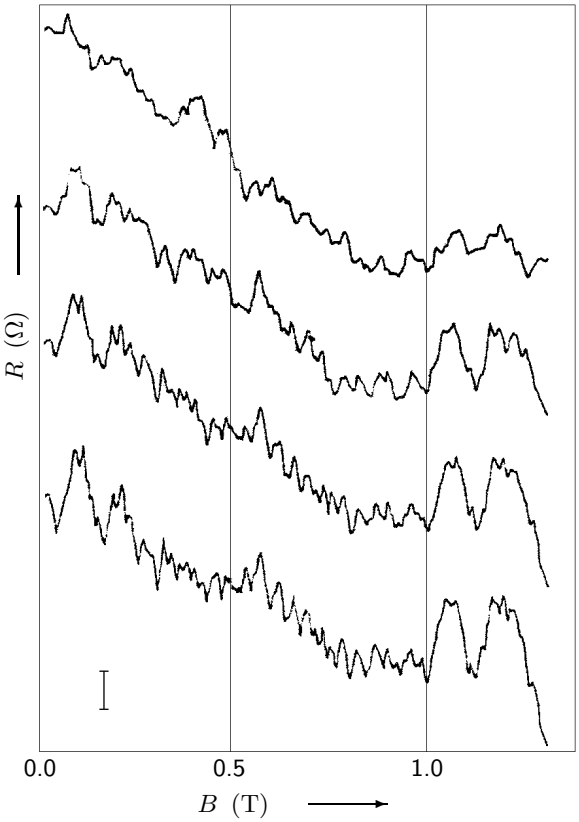

Fig. 264: MR data of a GaAs ring [87I2] for different temperatures. From the top, the zero–field resistances and the temperatures are: 4400 Ω, 4.2 K; 4440 Ω, 3.1 K; 4420 Ω, 2.3 K; 4480 Ω, 1.5 K. The vertical bar denotes an amplitude of 100 Ω.

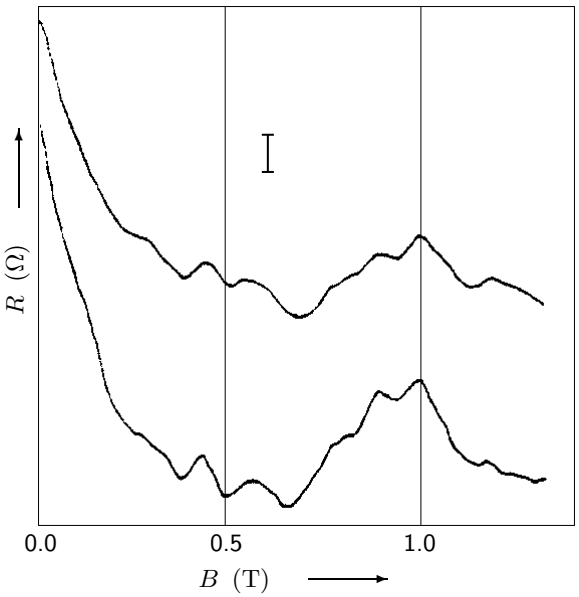

Fig. 265: MR data of a ring with one arm intentionally cut [87I2] for two different temperatures. From the top, the zero–field resistance and the temperature are: 10.0 kΩ, 4.2 K; 10.7 kΩ, 1.5 K. The vertical bar denotes an amplitude of 200 Ω.

Mankiewich et al [88M2] reported AB oscillations in rings fabricated by EBL and RIE in modulation–doped GaAs. The devices had $0.5\,\mu$m wide channels, resulting in electrical widths from 0.06 to $0.22\,\mu$m. The ring diameter measured between the centres of the channels was $1.9\,\mu$m. Data for R_L and R_H are shown in Fig. 267. The modulation of the total resistance of the sample due to the oscillations was about 10%. Periodic oscillations were found in R_H, indicating that interference effects from the entire geometry of the conducting path influenced the conductance.

Chang et al [88C5] studied a GaAs/AlGaAs heterostructure ring patterned by EBL and RIE. The lithographic linewidth was 500 nm, the conducting width was 200 ± 20 nm. The elastic scattering length was ≈ 400 nm, the path between the voltage probes was $3.5\,\mu$m long. The MR, R_L and R_H, at 50 mK is shown in Fig. 268. A large negative MR in R_L was observed for $-0.3\,\mathrm{kG} < B < 0.3\,\mathrm{kG}$ (Fig. 269). At $T = 4\,\mathrm{K}$ and $B = 0\,\mathrm{T}$, the negative MR peak was about 7% larger than the background resistance; at 50 mK it was 90% larger. At higher fields, AF and quasi–periodic fluctuations (QF) were observed in R_L, AF were observed in R_H. In Fig. 270, QF

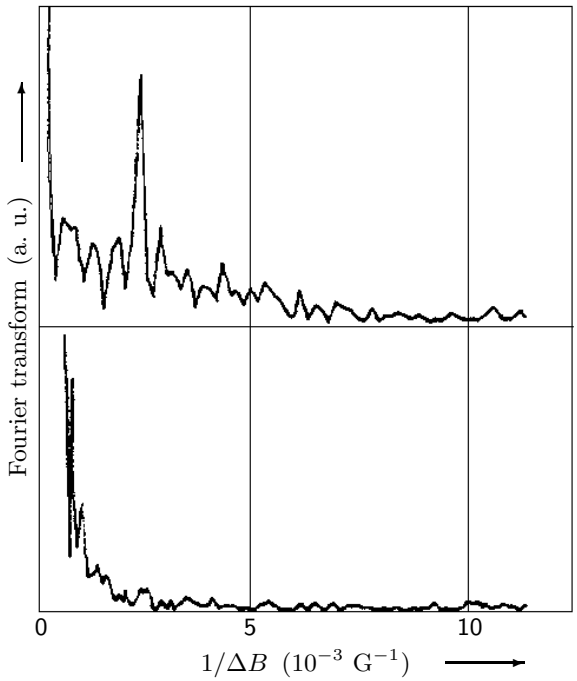

Fig. 266: Fourier transform of the MR data of the ring (top, see Fig. 264) and the broken ring (bottom, see Fig. 265) as found in [87I2]. The period of the h/e oscillations was about 400 G. The Fourier transform of the broken ring shows no peak but only AF.

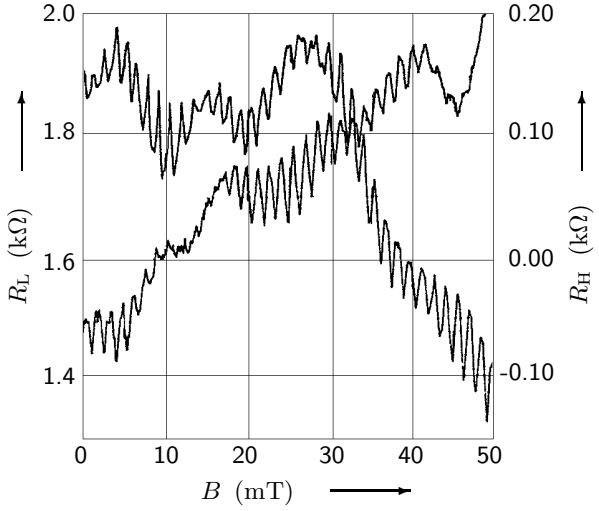

Fig. 267: Longitudinal MR and Hall resistance of a GaAs ring at 300 mK [88M2]. The curve with the larger resistance at $B = 0$ T is R_L (left axis), the other curve is R_H (right axis).

with an average period of 55 G are displayed, 52 G would have been expected for the AB effect. Between 4 and 7.1 kG, the fluctuations in R_L at 150 mK showed a large amplitude component which was almost periodic (period $\approx$ 400 G). Chang et al interpreted these oscillations as structural resonances as electron waves scattered from geometrical features in the device. They finally studied the temperature dependence of the h/e AB oscillations and the AF. The amplitude of the AF and the QF in R_L was comparable to that of the AF in R_H between 50 mK and 4 K and followed roughly a $T^{-0.75\pm0.25}$ law between 150 mK and 4 K. Further, the relative size of the AF and the QF component of R_L in comparison with the negative MR peak depended on temperature. At high T, the negative MR peak was favoured. The phase coherence length was $0.66 \cdot (T/2\mathrm{K})^{-0.35}\,\mu$m.

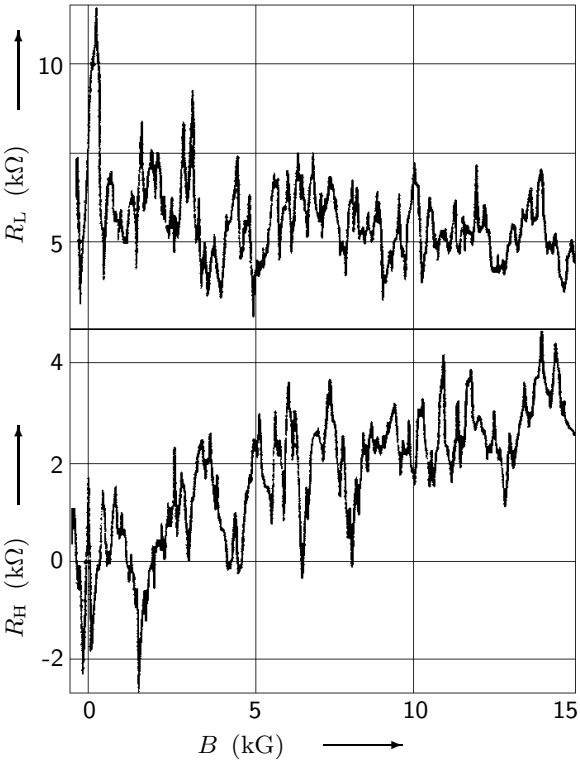

Fig. 268: R_L (top) and R_H (bottom) vs. magnetic field for a single ring at $T = 50$ mK [88C5].

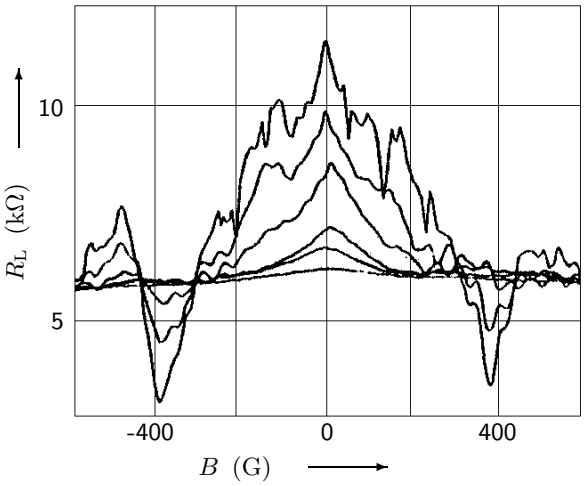

Fig. 269: MR peak in R_L for (from the top of the MR peak) $T = 50$ mK, 150 mK, 250 mK, 600 mK, 1.5 K, and 4.0 K [88C5].

Simmons et al [88S3] (see page 168) performed MR measurements (at $T = 0.3$ K) on doubly connected rings ($w \approx 1\,\mu$m, $L = 25\,\mu$m) and standard Hall bridges ($w \approx 1\,\mu$m, $L = 2\,\mu$m) made from GaAs/Al_xGa_{1-x}As heterostructures. They observed h/e AB oscillations in the rings. Samples of both geometries showed resistance fluctuations.

Scherer et al [87S1] (see page 201) patterned GaAs wires and rings by low–energy ion etching. They observed AB oscillations in the rings.

Ford et al [88F3] (page 259) studied MR in GaAs rings and observed AB oscillations (Figs. 255 and Fig. 256). They did not decrease in amplitude up to fields between 0.5 and 1 T, depending on the channel width.

De Vegvar et al [88dV] (page 273) studied h/e AB oscillations in small rings fabricated from GaAs/Al_xGa_{1-x}As heterostructures. The oscillations were suppressed as the magnetic field increased and vanished above ≈ 0.9 T.

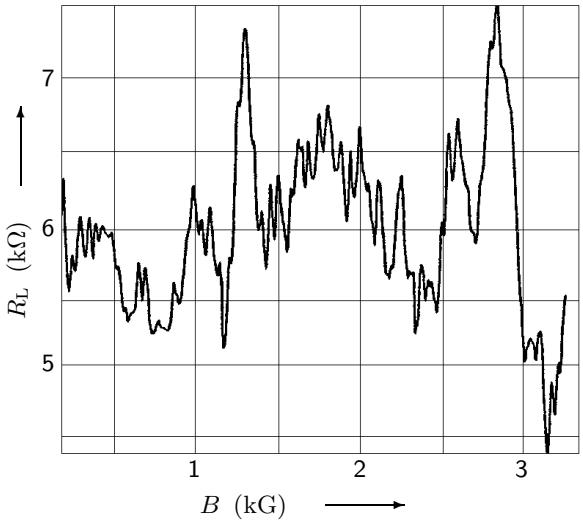

Fig. 270: QF in R_L at 150 mK in a GaAs ring [88C5].

Ford et al [89F3] (page 259) reported relative amplitudes of AB oscillations as large as 20% in a GaAs ring structured by electrostatic confinement. By filtering the MR data, $h/2e$ oscillations were also found, which behaved similar to the h/e oscillations for $B \geq 4\,\mathrm{mT}$. For smaller magnetic fields, they showed characteristic features of the weak–localization oscillations. The period of the AB oscillations increased sharply as B was swept from zero to $\approx 0.3\,\mathrm{T}$. The overall increase in period was 25% and indicated a decrease in the average area enclosed by the ring.

Timp et al [89T7] studied the suppression of the AB effect in the quantized Hall regime. The devices made of AlGaAs/GaAs were defined by an etch mask patterned by EBL. The lithographic diameter of the loop was $1.82 \pm 0.05\,\mu\mathrm{m}$, the linewidth was 500 nm, and the conducting width was estimated to be $< 25\,\mathrm{nm}$. The four–terminal MR is shown in Fig. 271. Superimposed upon background fluctuations, h/e AB oscillations were found around 0 mT which decreased in amplitude and frequency for a growing magnetic field. An $h/2e$ oscillation was also observed, a phase coherence length $> 3\,\mu\mathrm{m}$ was deduced. The peak in the Fourier transform decayed exponentially with magnetic field for $200\,\mathrm{mT} < B < 1.6\,\mathrm{T}$. The centre of the power spectrum shifted from $630\,\mathrm{T}^{-1}$ to $420\,\mathrm{T}^{-1}$ near 1 T. The radius corresponding to $420\,\mathrm{T}^{-1}$ was $\approx 0.75\,\mu\mathrm{m}$, which was greater than the inside lithographic radius by 70 nm. The spectral position of the peak did not depend on magnetic field for $1\,\mathrm{T} < B < 2.5\,\mathrm{T}$. The peak in the spectra near $420\,\mathrm{T}^{-1}$ found for $B > 800\,\mathrm{mT}$ vanished near the resistance minima in R_L, but reappeared beyond the minima. The minima observed in R_L corresponded to plateaux in R_H. Timp et al interpreted the suppression of the AB effect to be due to the absence of backscattering between edge states which carry the current for fields for which $w \approx 2r_c$.

Takagaki et al [89T6] studied the phase coherence length in arrays of few GaAs wires and compared the amplitude of AB oscillations in a ring fabricated of the same wafer with predictions following from the measured l_φ (see page 230).

De Vegvar et al [89dV] (page 274) examined a tunable electron interferometer in which a gate was constructed over one branch of the ring. The AB effect caused MR oscillations with a relative amplitude of up to 10%. The interference condition could be altered via a negative voltage applied across the gate. A phase shift of the AB oscillations occurred when the gate voltage was changed from 0 to −300 mV (Fig. 279). As no periodic structure in the resistance as a function of V_g was found, the phase shifts were attributed to a shift in the Feynman trajectories.

Behringer et al [89B2] (see page 176) fabricated GaAs wires and rings (diameter $2\,\mu\mathrm{m}$, $w_{\mathrm{eff}} \approx 200\,\mathrm{nm}$) by shallow etching and observed AB oscillations in the MR of the rings.

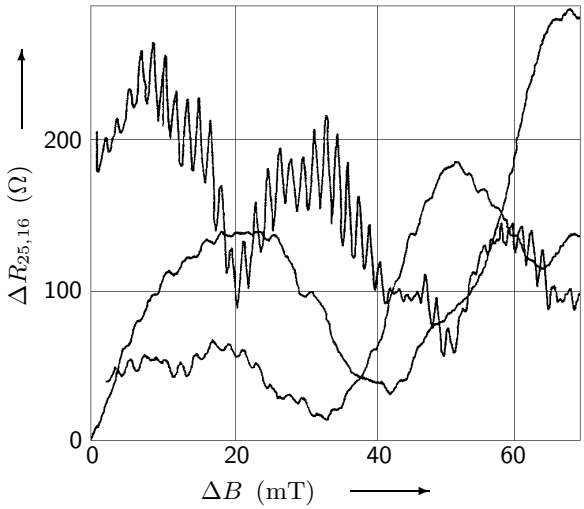

Fig. 271: Four–terminal MR, $R_{25,16}$, at 280 mK near (top at $\Delta B = 10$ mT) 0 mT, 2.47 T, and 0.92 T (bottom at $\Delta B = 10$ mT) [89T7].

Ford et al [90F5] (page 274) examined rings in which the phase difference could be tuned by changing the electron wavelength via a metal gate. For rings with arms of different lengths, the path difference $k_F \Delta L$ could be varied by changing V_g. AB oscillations in the MR (up to a relative amplitude of 50%) were observed. They studied the effects of a change in k_F. Another asymmetric ring had the form of a D. The AB oscillations had a relative amplitude $\leq 20\%$ and died out at relatively low fields, $B \leq 0.2$ T. The oscillations were fairly symmetric about $B = 0$ T, the phase appeared to be pinned at $B = 0$, thus a clear variation with V_g was not observed.

Smith et al [90S] (see page 233) investigated a GaAs device with a grid–like conducting structure consisting of 0.5 μm long 1D ballistic channels connected both parallel and in series and observed AB oscillations.

Aihara et al [91A3] (page 255) studied MR in a GaAs ring, data for various temperatures is shown in Fig. 246. In the Fourier transform of the data at 0.75 K (Fig. 247), peaks corresponding to h/e and $h/2e$ AB oscillations were present.

Ismail et al [91I2, 91L1] reported AB oscillations in arrays of rings fabricated by high–resolution EBL and wet chemical etching from high–mobility GaAs/AlGaAs modulation–doped heterostructures. The electron mean free path was $4 - 5\,\mu$m. The arrays consisted of one, two, and four coupled parallel rings of 1.25 μm inner diameter and 1.65 μm outer diameter. AB oscillations in single and parallel rings were observed at $T = 0.1$ K, see Fig. 272 for the two–loop sample. The amplitude of the oscillations increased with V_g for a positive gate bias above threshold, reached a maximum and decreased again. The positions of the maxima were at resistance values of 15, 7 and 4 kΩ in the one–, two– and four–ring arrays, respectively. The largest conductance modulation was observed in the two–loop samples and when the loops contained only a single mode, also the four–ring sample showed larger AB oscillations than the single loop. Further, the conductance of the rings showed a step–like behaviour as a function of gate voltage at 4.2 K. When recycling the gate bias, the threshold voltage shifted by ≈ 50 mV, the height of the steps was unaltered. In the single ring, the height of the steps was $0.8 \cdot e^2/h$, in the two–loop sample it was $1.2 \cdot e^2/h$, see Fig. 273. Similar steps were observed in $2 - 4\,\mu$m long single wires as well as in ten parallel wires. The step height in the single wires was $2 \cdot e^2/h$ and it was $20 \cdot e^2/h$ in the parallel wires.

Kurdak et al [92K1] (page 256) studied AB interference effects in rings and wire arrays of $GaAs/Al_{0.3}Ga_{0.7}As$ and pseudomorphic $Ga_{0.2}In_{0.8}As/Al_{0.48}In_{0.52}As$ modulation–doped heterostructures. MR data for a 7.8 μm perimeter ring of GaAs and a 5.2 μm perimeter ring of GaInAs at different temperatures are shown in Figs. 250 and 251. The AB oscillations had the expected h/e period.

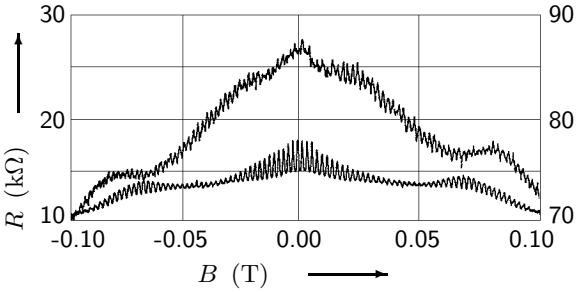

Fig. 272: MR data of the two–loop sample [91I2] at $T = 0.01\,\mathrm{K}$ for a gate voltage of 0.15 V (lower curve, left axis) and for 0.075 V (upper curve, right axis).

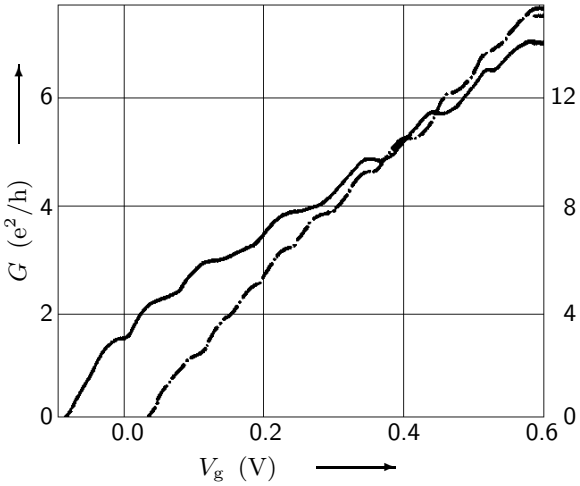

Fig. 273: Conductance as a function of gate voltage at $T = 4.2\,\mathrm{K}$ in the single ring (solid curve, left axis, x-axis shifted by $-0.1\,\mathrm{V}$) and in the two–ring sample (dash–dotted curve, right axis) [91I2].

Mailly et al [93M1, 94M1] (see page 252) observed AB oscillations in the GaAs rings in which they studied PCs.

Okuda [93O4] (page 260) observed AB oscillations in the MR of a GaAs double–wire interferometer.

Liu et al [94L2] studied coupled rings fabricated from modulation–doped GaAs/$Al_{0.3}Ga_{0.7}As$ defined by a shallow mesa and entirely covered with a gate. The samples consisted of four coupled rings with average lithographic radii of 0.48 μm and linewidths of 0.49 μm for the rings and 0.33 μm for the ports. The electrical widths of the conducting channels were about 0.1 μm narrower on each side due to depletion. All data was taken at $T = 0.04\,\mathrm{K}$. The MC at two different gate voltages is shown in Fig. 274. At low magnetic field, higher harmonics could occur because electrons encircled the ring more than once before interfering. At high fields, the AB effect arose from tunneling between the transport edge–states and the interior localized states. A possibility for higher harmonic generation was multiple tunneling through several localized states. The fundamental peak shifted from $\approx 190\,\mathrm{T}^{-1}$ to $\approx 135\,\mathrm{T}^{-1}$ as the magnetic field increased from 0 T to 2.5 T. The shift was due to the fact that less area was enclosed by the edge–states. Further, Liu et al reported that the phase coherence length increased with B. The amplitude of the h/e AB oscillation, $\langle \Delta G(B) \rangle$, was expected to scale as $Pe^{-\Delta l/l_\varphi}$, with P the interference probability of the two partial waves, and Δl the distance a wave travels before the interference. An increase in $\langle \Delta G(B) \rangle$ with magnetic field indicated an increase in l_φ.

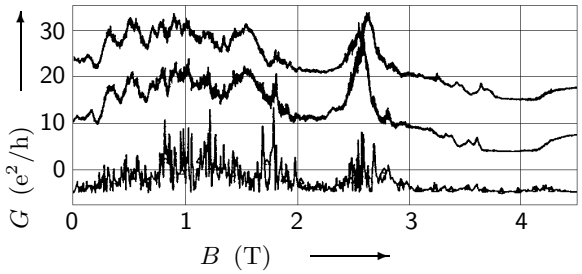

Fig. 274: MC at gate voltages of 0.7 V (top, offset by $10 \cdot e^2/h$) and 0.695 V (middle). The bottom curve is the amplitude $\langle \Delta G(B) \rangle$ of the h/e AB oscillations at $V_g = 0.695\,\mathrm{V}$ (amplified by 10 and offset by $-5 \cdot e^2/h$) [94L2].

Gao et al [94G1] reported the first observation of the AB effect in the MR of Si/SiGe rings. The experiment was performed at 0.04 K. A typical MC and the corresponding Fourier transform are shown in Figs. 275 and 276. The fundamental h/e frequency and the first and second harmonic frequencies were $151.7\,\mathrm{T}^{-1}$, $319.1\,\mathrm{T}^{-1}$, and $\approx 470\,\mathrm{T}^{-1}$. From the h/e frequency, a radius of the ring of $0.45\,\mu$m was deduced. The lithographic radius was $0.42\,\mu$m. A phase coherence length of $1.2 \pm 0.7\,\mu$m was inferred, see the inset of Fig. 276. The AB oscillations persisted up to ≈ 0.35 T. In an array of four parallel rings made of a Si/SiGe heterostructure, Gao et al observed conductance steps. A plot of the conductance vs. gate voltage at ≈ 1 K is shown in Fig. 277. The steps were not exactly equally spaced, their origin was not absolutely clear.

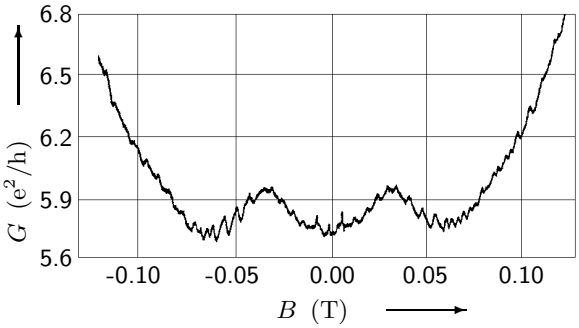

Fig. 275: MC of a single Si/SiGe ring [94G1].

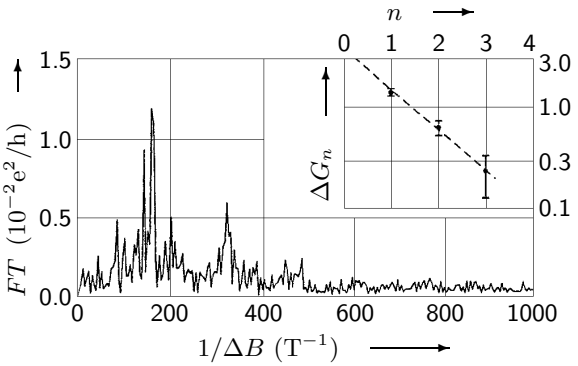

Fig. 276: Fourier transform of the data in Fig. 275. Inset: The average AB oscillation amplitudes ΔG_n in units of $10^{-3} \cdot e^2/h$ as a function of the harmonic index n in order to determine l_φ. The fit to the amplitudes is the dashed line.

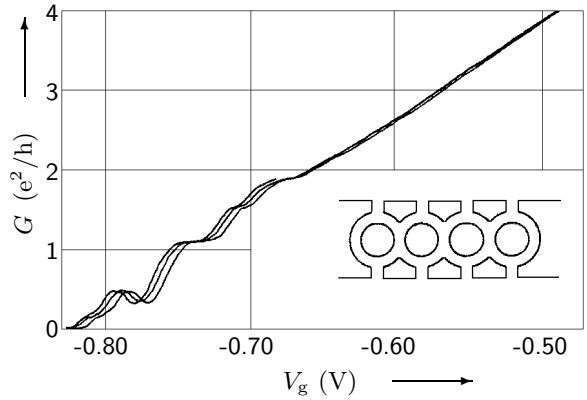

Fig. 277: Conductance vs. gate voltage at $T > 1$ K for the array of rings [94G1] illustrating the step–like features at $B = 0$ T. Several traces were made while the threshold was drifting (soon after cooling) to show the reproducibility of the features. The inset is a plan view of the four coupled rings.

Appenzeller et al [95A2] (page 258) investigated MR in rings of small width in a strained $In_{0.77}Ga_{0.23}As/InP$ system. The four–terminal MR, R_L, as a function of magnetic field at 330 mK is shown in Fig. 253. The AB oscillations had an amplitude of $1\,\mathrm{k}\Omega$ on a background resistance of $8.5\,\mathrm{k}\Omega$.

Yacoby et al [95Y2] (page 260) constructed a GaAs ring with a QD embedded in its left side arm. MR was measured at $T = 80$ mK, AB oscillations were observed, directly indicating that transport through the QD had a coherent component (Fig. 258). AB oscillations for three typical successive CB peaks had all the same phase at the peaks (Fig. 259). Following the phase along a single CB peak, a phase change of π occurred (Fig. 260).

Bykov et al [95B3] (page 264) structured GaAs rings and performed MR measurements. At small B, a negative MR was observed, AB oscillations were superimposed on the negative MR. At large B, the MR exhibited plateaux. The MR for $0.6 < \nu < 0.65$ also exhibited AB oscillations while for $\nu = 1/2$, no MR oscillations were present.

Park et al [96P2, 96P3] (page 275) fabricated and studied a GaAs ring with two metal gates of different length on top of both arms. In the MR spectrum, two sets of h/e oscillations, almost equal in magnitude and shifted by π with respect to each other, were observed (Fig. 281). They attributed the observed phenomena to the magnetostatic and the electrostatic AB effects occurring simultaneously.

Morpurgo et al [98M] (page 262) searched for a manifestation of Berry's phase via a splitting of the frequency of AB oscillations. They fabricated rings from a AlSb/InAs/AlSb heterostructure. The AB effect was measured at 100 mK. The peak in the Fourier spectrum appeared at h/e.

10.7 Non–linear effects

For an introduction see Section 7.9 on page 210.

De Vegvar et al [88dV] studied second harmonic generation in small rings and wires fabricated from GaAs/Al_xGa_{1-x}As heterostructures. The conducting channel width was $w \approx 100$ nm, which was larger than the Fermi wavelength. The devices were quasi–ballistic with $2-3$ 1D channels occupied. The material for ring 1 (2) was characterized by an elastic scattering length of $l = 2.7\,\mu$m ($l_\varphi \geq 4\,\mu$m, $l \approx 6.4\,\mu$m), $w = 90-110$ nm ($w \approx 100$ nm), and $L \approx 5\,\mu$m ($L \approx 5\,\mu$m) at $T = 280$ mK. In both ring samples, h/e AB oscillations were detected which were suppressed as the magnetic field increased and vanished above ≈ 0.9 T. A sinusoidal current at $f = 11$ Hz was injected in order to observe non–linearities. Results for $V(nf)$ as a function of $I(f)$ for $n = 2$, and 3 in material 2 are shown in Fig. 278. At $I = 1$ nA, it was $|V(2f)/V(f)| \approx 3 \times 10^{-4}$ and $|V(3f)/V(f)| \approx 1 \times 10^{-3}$. For a current drive > 1 nA, deviations from $V(2f) \propto I^2$ and $V(3f) \propto I^3$ were observed. Harmonics up to $10{\cdot}f$ have been detected. De Vegvar et al believed that the source of the non–linearity was quantum interference.

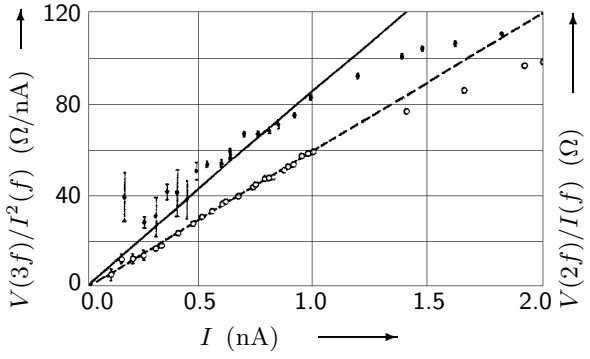

Fig. 278: Second (open symbols, right axis) and third (closed symbols, left axis) harmonic generation as a function of the applied ac current in material 2 [88dV]. The data obeyd the law $V(nf) \propto I^n(f)$ as shown by the dashed and solid lines for $n = 2$ and 3, respectively.

Chandrasekhar et al [94C1] (page 275) investigated InO rings and wires and found non–linear I–V characteristics. The application of a magnetic field affected the non–linear I–V characteristic of the wires, as can be seen in Fig. 290, where a wire has been examined at 102 mK for four different magnetic fields.

10.8 Electrostatic Aharonov–Bohm effect

An electric field may cause a phase shift in probability amplitudes, $\Delta\varphi_j = (e/\hbar)\int V(t)dt$, where V is the scalar potential an electron is subject to on its path and the integral is taken over the period of time the electron spends in contact with V. Resulting periodic oscillations in the transmission probability of the ring as a function of V are known as the *electrostatic* AB effect (see also Section 10.6.2 on page 264). In addition, an electric field penetrating the material of a ring of finite cross-section shifts the positions of the electrons. By the resulting rearrangement of the trajectories, the interference pattern and hence the conductance are altered (see for example [89W2, 91W2] and references therein).

De Vegvar et al [89dV] examined a tunable electron interferometer fabricated from high–mobility GaAs/Al_xGa_{1-x}As heterostructures. The annuli were patterned by EBL and RIE, the ring diameter was 1.88 μm, and the effective conducting width was $90 - 130$ nm. A 0.3 μm wide AuPd gate was constructed over one branch of the ring. The Fermi wavelength was ≈ 60 nm, the elastic scattering length was $1.6 - 2.0\,\mu$m, the rings mean circumference was 5.9 μm, and the phase coherence length was $\geq 5\,\mu$m. Only $2 - 3$ subbands were occupied. The AB effect caused MR oscillations with a relative amplitude of up to 10%. The interference condition could be altered via a negative voltage applied across the metal gate. A phase shift of the AB oscillations occurred when the gate voltage was changed from 0 to -300 mV (Fig. 279). The phase shift was reversible when V_g returned to zero. The influence of larger variations of V_g on the AB effect is shown in Fig. 280. As no periodic structure in the resistance as a function of V_g was found, the phase shifts were attributed to a shift in the Feynman trajectories.

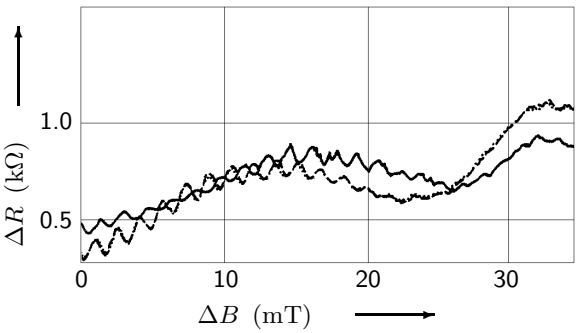

Fig. 279: MR of the gated 1.88 μm diameter ring [89dV]. The dashed curve was recorded with $V_g = 0$ mV first, V_g was then swept to -300 mV, producing the solid trace. The dotted data refer to data obtained when V_g was returned to zero.

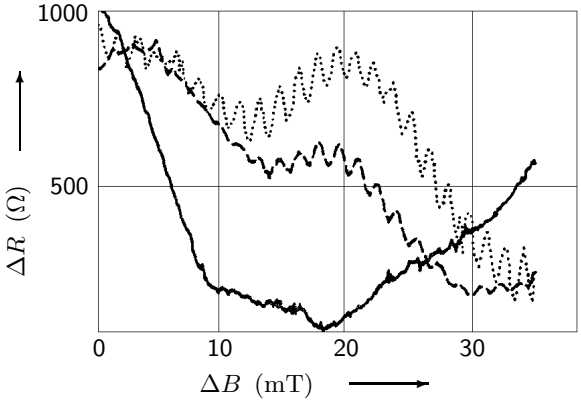

Fig. 280: MR traces taken of the same sample as in Fig. 279 over a wider range of V_g. The gate voltage is $V_g = -2000$ mV for the solid, -700 mV for the dashed, and 0 mV for the dotted curve.

Ford et al [90F5] examined rings in which the phase difference could be tuned by changing the electron wavelength via a metal gate. The starting material was a GaAs/Al_xGa_{1-x}As heterostructure, the ring was patterned by EBL and RIE. The device was then covered with an Au gate, allowing the carrier concentration and the channel width to be varied. It was $w \approx 100$ nm and $n \approx 1 \times 10^{15}\,\mathrm{m}^{-2}$ near pinch off, the Fermi wavelength was $50 - 80$ nm. At the lowest V_g, $2 - 3$ subbands were occupied. For rings with arms of different lengths, the path difference $k_F\Delta L$ could be varied by changing V_g. The first asymmetric ring was a rectangle with leads attached close to the bottom of the longer sides. The difference in path lengths between the two arms of the ring was nominally 1 μm. At 25 mK, AB oscillations in the MR up to a relative amplitude of 50% were

observed. Ford et al studied the effects of a change in k_F. The oscillations seemed to have the same phase over a wide range of V_g. Reducing V_g in order to obtain a single occupied band caused some parts of the channels to pinch off before others due to lithographic imperfections. Another asymmetric ring had the form of a D. The path difference was 1 μm, the circumference was 2.7 μm. Different leads pinched off at different gate voltages. Three rings of that kind were investigated at $T < 35$ mK. The AB oscillations had a relative amplitude $\leq 20\%$ and died out at relatively low fields, $B \leq 0.2$ T. The oscillations were fairly symmetric about $B = 0$ T, the phase appeared to be pinned at $B = 0$, thus a clear variation with V_g was not observed.

Bykov et al [94B1] measured the influence of an electrostatic field on electron interference effects in submicron GaAs/AlGaAs rings by coupling a microwave to the ring. In [93B5] , Bykov et al had already demonstrated that the AB effect could be observed via the mesoscopic photovoltaic effect (see page 291). In samples very similar to those studied in [94B1], Bykov et al eventually found aperiodic and periodic components in the voltage (induced by the microwave field) as a function of gate voltage [95B4] (see page 291). Later, Bykov et al [96B2] (see page 291) investigated in–plane gated InGaAs/AlGaAs rings, measured MR in a four–probe geometry and determined the influence of V_g on the properties of the rings by using again the microwave photovoltaic effect.

Park et al [96P2, 96P3] fabricated and studied a GaAs ring with two metal gates of different length on top of both arms. The ring of average diameter 1.9 μm and conduction width 0.3 μm was structured by EBL and chemical etching on a modulation–doped GaAs/$Al_{0.3}Ga_{0.7}As$ heterostructure. The distance between the measuring leads was 3.8 μm. The length of the Au/Ni gate was 0.2 μm on one arm of the ring and 1 μm on the other. In the MR spectrum, two sets of h/e oscillations, almost equal in magnitude and shifted by π with respect to each other, were observed (Fig. 281). For $-40\,\mathrm{G} < B < 40\,\mathrm{G}$, the peak positions did not change with V_g, but the amplitudes did. At $V_g = -195.3$ mV, additional oscillations began to appear. The magnitudes of the oscillations became almost equal at -206.2 mV. The variation in amplitude of the two oscillations with V_g as deduced from the data in Fig. 281 can be seen in Fig. 282. Park et al attributed the observed phenomena to the magnetostatic and the electrostatic AB effects occurring simultaneously.

10.9 Dispersion relation

Liu et al [93L3] studied the dispersion relation in rings fabricated from a GaAs/$Al_xGa_{1-x}As$ modulation–doped layer. The ring geometry was defined by wet etching. The ring had a radius of 0.85 μm and a linewidth of 0.3 μm. The experiments were performed at 4.2 K. The conductance G of the ring as a function of the gate voltage at $B = 0$ T is shown in Fig. 283. The regularly spaced conductance steps indicated the number of current carrying modes, the average height of the steps was $0.75 \cdot e^2/h$. The MR is displayed in Fig. 284, peaks occurred when the cyclotron radius, r_{cn}, of the n-th band matched the ring radius. As r_{cn} was related to the Fermi wave vector, k_{F_n} could be deduced from the peak positions. Via the SdH effect, Liu et al obtained the Fermi level as a function of gate voltage, $E_F = 5.98 \cdot V_g + 12.4$ meV. As a function of the peak position (upper axis) and versus the wave vector (lower axis), E_F is displayed in Fig. 285. The data was compared with theoretical results concerning the dispersion relation of straight wires. The effective mass as a function of magnetic field was deduced and an enhancement of m^* with B was found.

10.10 Indium oxide rings

The rings and wires investigated by Chandrasekhar et al [94C1] consisted of In_2O_{3-x} with an electrically isolated gate electrode. The ring diameter was 0.3 μm, the gates were separated by ≈ 100 nm from one arm of the ring, the width of the wires varied from 30 to 150 nm. The two–terminal conductance measurements were performed at temperatures down to 40 mK in magnetic fields up to 12 T. The typical low temperature zero dc–bias resistance of the samples was $\approx 10^{11}\Omega$.

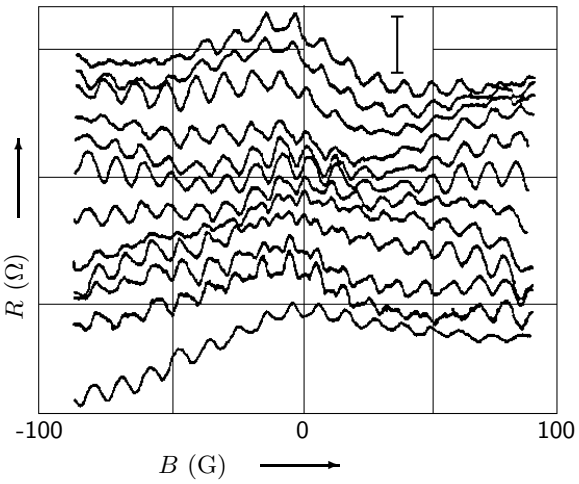

Fig. 281: Changes of the new set of h/e AB oscillations [96P2]. The difference in V_g between the successive curves was ≈ 4 mV. The curve at the top is at $V_g = -238.2$ mV, the one at the bottom at -195.3 mV. The vertical bar denotes an amplitude of $100\,\Omega$.

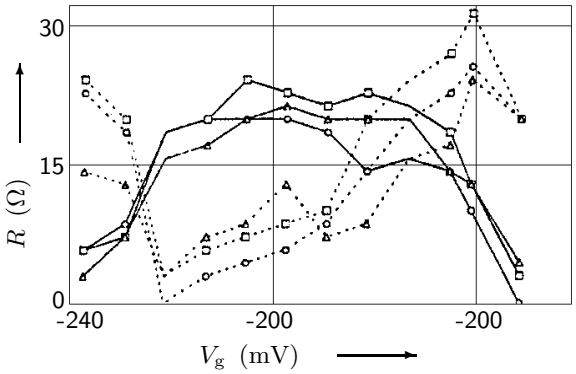

Fig. 282: The resistance changes of the amplitude of the new and the background h/e peaks vs. gate voltage [96P2]. The solid lines illustrate the changes when $B = -19$ G (circles), -8 G (boxes), and 3 G (triangles) for the new h/e peaks and the dotted lines are the changes when $B = -13$ G (circles), -3 G (boxes), and 7 G (triangles) for the background h/e peaks.

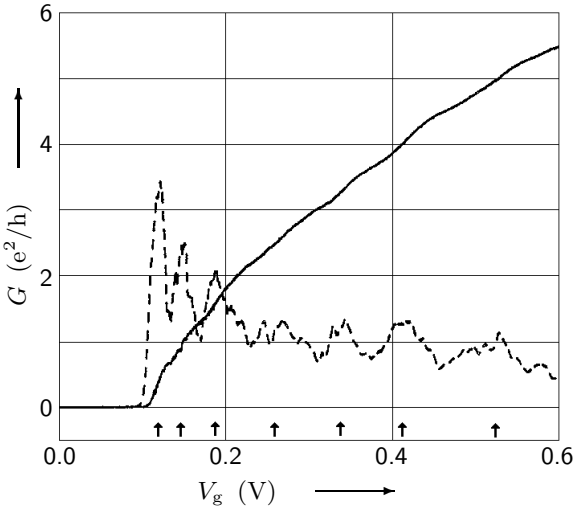

Fig. 283: Conductance vs. gate voltage [93L3]. The turn–on voltages for the modes are determined from dG/dV_g (dashed line) and marked by arrows. The first mode is the one most to the left, the one most to the right is the seventh mode.

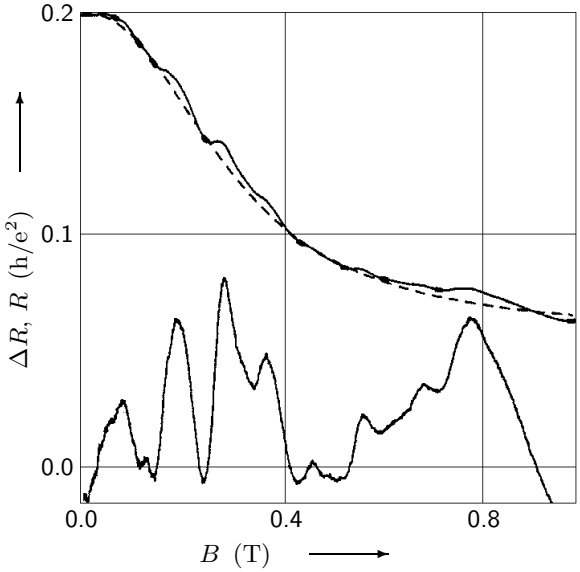

Fig. 284: MR of the ring [93L3] at $V_g = 0.55$ V (solid line) and smooth background (dashed line). The difference between the two, ΔR, results from orbit trapping.

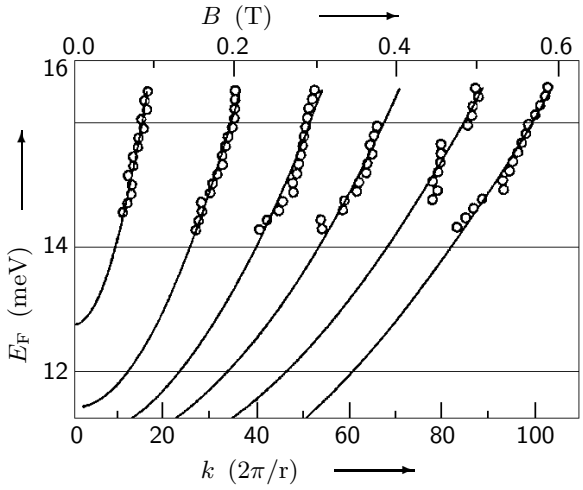

Fig. 285: The focussing peak positions for subband indices $2-7$ [93L3]. The solid curves are fits.

The conductance showed periodic oscillations as a function of gate voltage with a period $\approx 20\,\mathrm{mV}$ for a special sample. The oscillations persisted up to gate voltages of $\pm 10\,\mathrm{V}$ and temperatures of 12 K in some samples. When the temperature decreased, the amplitudes of the minima of the oscillating conductance vanished while the amplitudes of the maxima were at first reduced and became relatively constant at low temperatures (Fig. 286). The period of oscillation did not change with temperature. In other samples, the amplitude of some peaks decreased that fast when temperature was lowered that the oscillation pattern appeared to be aperiodic (Fig. 287). In a straight wire of indium oxide, conductance oscillations as a function of gate voltage were also observed. Both, the amplitude of the conductance maxima as well as of the conductance minima became temperature independent at a finite value of conductance at low temperature. The conductance oscillations observed in the ring samples thus seemed not to be due to the doubly connected structure of the rings, as a straight wire showed similar oscillations. Even though the oscillations of the conductance as a function of gate voltage were in general reproducible if the sample was kept at low temperature, the conductance of a sample occasionally changed in a discrete way, usually accompanied by a change in the pattern of the oscillations; the period of the oscillations was not affected. Chandrasekhar et al believed the discrete behaviour of the conductance to be due to the movement of isolated impurities. Many of the observed phenomena could be accounted for the physics of the Coulomb blockade. The conductance oscillations as a function of gate voltage for a ring sample for various values of magnetic field from $B = 0\,\mathrm{T}$ to $B = 9.25\,\mathrm{T}$ are shown in Fig. 288. The positions of the conductance maxima with respect to the gate voltage shifted as a function of magnetic field and some of the detailed structure changed. The period of the oscillations remained constant to within 3% over the entire magnetic field range. Similar traces for a narrow wire at 40 mK are shown in Fig. 289. The period of the oscillations varied by more than 40%. The application of a magnetic field also affected the dc current–voltage characteristic of the indium oxide wires, as can be seen in Fig. 290, where a wire has been examined at 102 mK for four different magnetic fields.

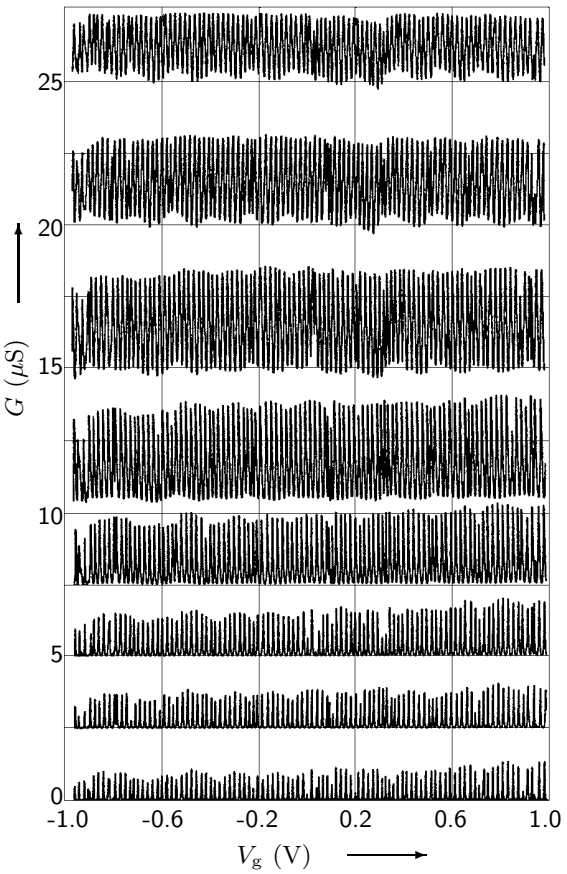

Fig. 286: Conductance vs. gate voltage of a 60 nm linewidth ring at (top) $T = 651$ mK, 483 mK, 312 mK, 195 mK, 135 mK, 94.1 mK, 60.5 mK, and 40 mK (bottom) [94C1]. Traces have been offset from each other along the y-axis by 2.5 μS for clarity.

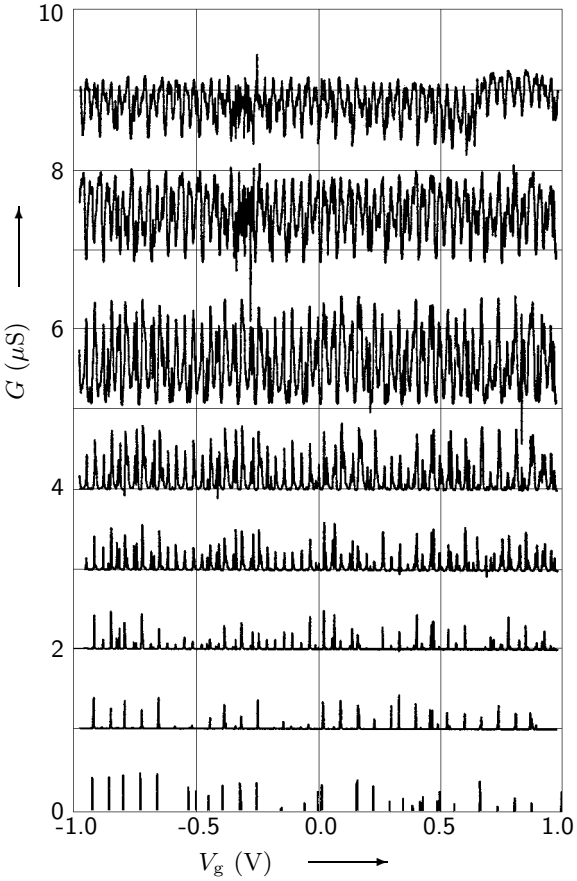

Fig. 287: Conductance vs. gate voltage of a 50 nm linewidth ring at (top) $T = 2.23$ K, 1.638 K, 939 mK, 505 mK, 333 mK, 215 mK, 126.8 mK, and 39.0 mK (bottom) [94C1]. Traces have been offset from each other along the y-axis by 1 μS for clarity.

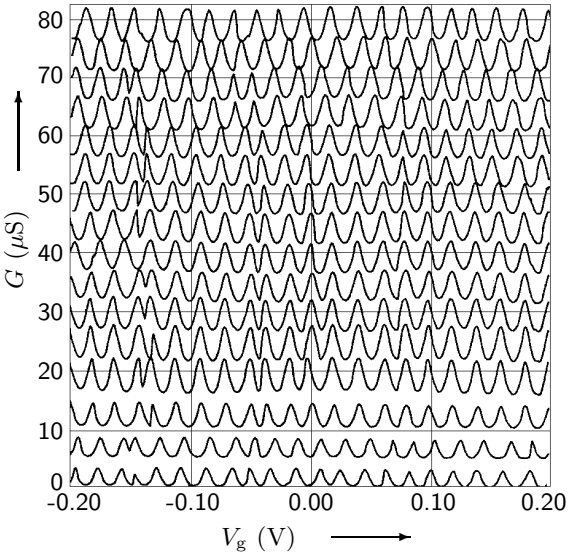

Fig. 288: Conductance vs. gate voltage for the ring sample of Fig. 286 at $T = 200\,\mathrm{mK}$ for (top) $B = 9.25\,\mathrm{T}$, $8.75\,\mathrm{T}$, $8.25\,\mathrm{T}$, $7.75\,\mathrm{T}$, $7.25\,\mathrm{T}$, $6.75\,\mathrm{T}$, $6.25\,\mathrm{T}$, $5.75\,\mathrm{T}$, $5.25\,\mathrm{T}$, $4.75\,\mathrm{T}$, $3.75\,\mathrm{T}$, $2.75\,\mathrm{T}$, $1.75\,\mathrm{T}$, $0.75\,\mathrm{T}$, $0.37\,\mathrm{T}$, and $0.00\,\mathrm{T}$ (bottom) [94C1]. Traces have been offset from each other by $5\,\mu\mathrm{S}$ for clarity.

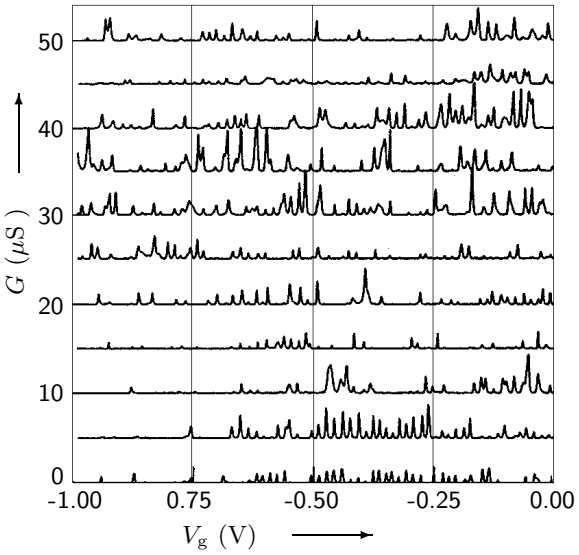

Fig. 289: Conductance vs. gate voltage for a straight wire at $T = 40\,\mathrm{mK}$ and (top) $B = 10.0\,\mathrm{T}$, $9.0\,\mathrm{T}$, $8.0\,\mathrm{T}$, $7.0\,\mathrm{T}$, $6.0\,\mathrm{T}$, $5.0\,\mathrm{T}$, $4.0\,\mathrm{T}$, $3.0\,\mathrm{T}$, $2.0\,\mathrm{T}$, $1.0\,\mathrm{T}$, and $0.0\,\mathrm{T}$ (bottom) [94C1].

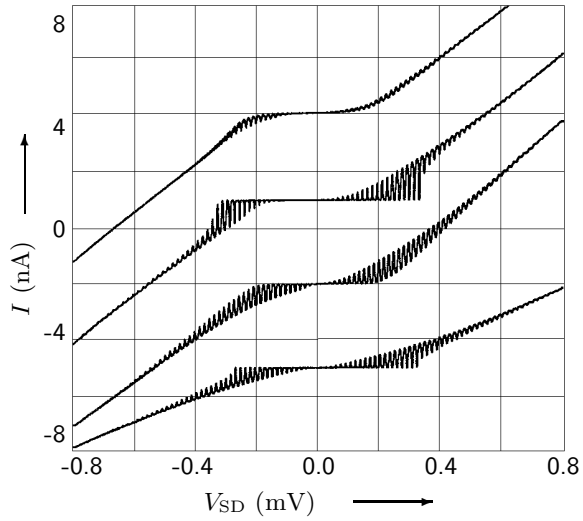

Fig. 290: dc I–V characteristic of the sample of Fig. 289 at (top) $B = 9\,\mathrm{T}$, $5\,\mathrm{T}$, $2\,\mathrm{T}$, and $0\,\mathrm{T}$ (bottom) [94C1]. The curves have been offset along the y-axis by $3\,\mathrm{nA}$ for clarity.

10.11 References for Section 10

[59A] Aharonov, Y., Bohm, D.: Phys. Rev. **115** (1959) 485.

[84B3] Berry, M.V.: Proc. R. Soc. London A **392** (1984) 45.

[86C1] Chakravarty, S., Schmid, A.: Phys. Rep. **140** (86) 193.

[86W1] Washburn, S., Webb, R.A.: Adv. Phys. **35** (1986) 375.

[87I2] Ishibashi, K., Takagaki, Y., Gamo, K., Namba, S., Ishida, S., Murase, K., Aoyagi, Y., Kawabe, M.: Sol. St. Commun. **64** (1987) 573.

[87S1] Scherer, A., Roukes, M.L., Craighead, H.G., Ruthen, R.M., Beebe, E.D., Harbison, J.P.: Appl. Phys. Lett. **51** (1987) 2133.

[87T1] Timp, G., Chang, A.M., Cunningham, J.E., Chang, T.Y., Mankiewich, P., Behringer, R., Howard, R.E.: Phys. Rev. Lett. **58** (1987) 2814.

[88C1] Chang, A.M., Timp, G., Chang, T.Y., Cunningham, J.E., Mankiewich, P.M., Behringer, R.E., Howard, R.E.: Sol. St. Commun. **67** (1988) 769.

[88C5] Chang, A.M., Timp, G., Chang, T.Y., Cunningham, J.E., Chelluri, B., Mankiewich, P.M., Behringer, R.E., Howard, R.E.: Surf. Sci. **196** (1988) 46.

[88dV] de Vegvar, P.G.N., Timp, G., Mankiewich, P.M., Cunningham, J.E., Behringer, R., Howard, R.E.: Phys. Rev. B **38** (1988) 4326.

[88F3] Ford, C.J.B., Thornton, T.J., Newbury, R., Pepper, M., Ahmed, H., Foxon, C.T., Harris, J.J., Roberts, C.: J. Phys. C: Solid State Phys. **21** (1988) L325.

[88K1] Kaplan, S.B., Hartstein, A.: IBM J. Res. Develop. **32** (1988) 347.

[88M2] Mankiewich, P.M., Behringer, R.E., Howard, R.E., Chang, A.M., Chang, T.Y., Chelluri, B., Cunningham, J., Timp, G.: J. Vac. Sci. Technol. B **6** (1988) 131.

[88S3] Simmons, J.A., Tsui, D.C., Weimann, G.: Surf. Sci. **196** (1988) 81.

[88T4] Timp, G., Chang, A.M., de Vegvar, P., Howard, R.E., Behringer, R., Cunningham, J.E., Mankiewich, P.: Surf. Sci. **196** (1988) 68.

[88W5] Webb, R.A., Washburn, S., Haucke, H.J., Benoit, A.D., Umbach, C.P., Milliken, F.P.: Physics and Technology of Submicron Structures, Solid–State Sciences 83, edited by Heinrich, H., Bauer, G., Kuchar, F. (Springer–Verlag, 1988).

[89B2] Behringer, R.E., Mankiewich, P.M., Timp, G., Howard, R.E., Baranger, H.U., Cunningham, J., Sampere, S.: J. Vac. Sci. Technol. **7** (1989) 2039.

[89dV] de Vegvar, P.G.N., Timp, G., Mankiewich, P.M., Behringer, R., Cunningham, J.: Phys. Rev. B **40** (1989) 3491.

[89F3] Ford, C.J.B., Thornton, T.J., Newbury, R., Pepper, M., Ahmed, H., Peacock, D.C., Ritchie, D.A., Frost, J.E.F., Jones, G.A.C.: Appl. Phys. Lett. **54** (1989) 21.

[89S4] Geometric Phases in Physics, edited by Shapere, A., Wilczek, F. (World Scientific, 1989).

[89T6] Takagaki, Y., Ishibashi, K., Ishida, S., Takaoka, S., Gamo, K., Murase, K., Namba, S.: Jpn. J. Appl. Phys. **28** (1989) 645.

[89T7] Timp, G., Mankiewich, P.M., de Vegvar, P., Behringer, R., Cunningham, J.E., Howard, R.E., Baranger, H.U., Jain, J.K.: Phys. Rev. B **39** (1989) 6227.

[89W1] Washburn, S.: Am. J. Phys. **57** (1989) 1069.

[89W2] Webb, R.A.: Nanostructure Physics and Fabrication, edited by Reed, M.A., Kirk, W.P. (Academic Press, inc., 1989).

[90D] Datta, S., McLennan, M.J.: Rep. Prog. Phys. **53** (1990) 1003.

[90F5] Ford, C.J.B., Fowler, A.B., Hong, J.M., Knoedler, C.M., Laux, S.E., Wainer, J.J., Washburn, S.: Surf. Sci. **229** (1990) 307.

[90S] Smith, C.G., Pepper, M., Newbury, R., Ahmed, H., Hasko, D.G., Peacock, D.C., Frost, J.E.F., Ritchie, D.A., Jones, G.A.C., Hill, G.: J. Phys.: Condens. Matter **2** (1990) 3405.

[91A3] Aihara, K., Yamamoto, M., Iwadate, K., Mizutani, T.: Jpn. J. Appl. Phys. **30** (1991) L1627.

[91I2] Ismail, K., Washburn, S., Lee, K.Y.: Appl. Phys. Lett. **59** (1991) 1998.

[91L1] Lee, K.Y., Kern, D.P., Ismail, K., Washburn, S.: J. Vac. Sci. Technol. B **9** (1991) 2834.

[91W2] Washburn, S.: Mesoscopic Phenomena in Solids, edited by Al'tshuler, B.L., Lee, P.A., Webb, R.A. (Elsevier Science Publishers B.V., 1991).

[92J2] Jin, G., Tang, Y.S., Thoms, S., Wilkinson, C.D.W., Gundlach, A.M.: J. Vac. Sci. Technol. B **10** (1992) 2873.

[92K1] Kurdak, C., Chang, A.M., Chin, A., Chang, T.Y.: Phys. Rev. B **46** (1992) 6846.

[92W1] Washburn, S., Webb, R.A.: Rep. Prog. Phys. **55** (1992) 1311.

[93B5] Bykov, A.A., Kvon, Z.D., Litvin, L.V., Nastaushev, Yu.,V., Mansurov, V.G., Migal', V.P., Moshchenko, S.P.: JETP Lett. **58** (1993) 543.

[93L3] Liu, J., Ismail, K., Lee, K.Y., Hong, J.M., Washburn, S.: Phys. Rev. B **47** (1993) 13039.

[93M1] Mailly, D., Chapelier, C., Benoit, A.: Phys. Rev. Lett. **70** (1993) 2020.

[93O4] Okuda, M.: Appl. Phys. Lett. **63** (1993) 3309.

[93O5] Okuda, M., Miyazawa, S., Fujii, K., Shimizu, A.: Phys. Rev. B **47** (1993) 4103.

[94B1] Bykov, A.A., Kvon, Z.D., Litvin, L.V., Moshchenko, S.P., Nastaushev, Yu., V.: JETP Lett. **60** (1994) 809.

[94C1] Chandrasekhar, V., Webb, R.A.: J. Low Temp. Phys. **97** (1994) 9.

[94G1] Gao, W.X., Ismail, K., Lee, K.Y., Chu, J.O., Washburn, S.: Appl. Phys. Lett. **65** (1994) 3114.

[94L2] Liu, J., Gao, W., Ismail, K., Lee, K., Hong, J., Washburn, S.: J. Low Temp. Phys. **97** (1994) 1.

[94M1] Mailly, D., Chapelier, C., Benoit, A.: Physica B **197** (1994) 514.

[95A2] Appenzeller, J., Schäpers, Th., Hardtdegen, H., Lengeler, B., Lüth, H.: Phys. Rev. B **51** (1995) 4336.

[95B3] Bykov, A.A., Kvon, Z.D., Ol'shanetskii, E.B., Litvin, L.V., Moshegov, N.T., Toropov, A.I.: JETP Lett. **62** (1995) 653.

[95B4] Bykov, A.A., Litvin, L.V., Moshchenko, S.P.: JETP Lett. **61** (1995) 1005.

[95Y2] Yacoby, A., Heiblum, M., Mahalu, D., Shtrikman, H.: Phys. Rev. Lett. **74** (1995) 4047.

[96B2] Bykov, A.A., Litvin, L.V., Moshchenko, S.P.: Surf. Sci. **361/362** (1996) 747.

[96K4] Kulik, I.O.: Physica B **218** (1996) 252.

[96P2] Park, K.W., Lee, S., Shin, M., Lee, E.-H., Kwon, H.C.: Phys. Rev. B **54** (1996) 1498.

[96P3] Park, K.W., Lee, S., Shin, M., Lee, E.-H., Kwon, H.C.: Surf. Sci. **361/362** (1996) 751.

[97F] Ferry, D.K., Goodnick, S.M.: Transport in Nanostructures (Cambridge University Press, 1997).

[97I1] Imry, Y.: Introduction to Mesoscopic Physics (Oxford University Press, 1997).

[98J1] Janssen, M.: Phys. Rep. **295** (1998) 1.

[98K6] Kvon, Z.D., Voronin, M.M., Kim, K., Lee, H.J.: JETP Lett. **67** (1998) 1029.

[98M] Morpurgo, A.F., Heida, J.P., van Wees, B.J., Klapwijk, T.M., Borghs, G.: Physica B **249-251** (1998) 509.